Unclassified
SECURITY CLASSIFICATION OF THIS PAGE

DTIC FILE COPY

REPORT DOCUMENTATION PAGE

1a. REPORT SECURITY CLASSIFICATION	1b. RESTRICTIVE MARKINGS
AD-A209 942	3 DISTRIBUTION/AVAILABILITY OF REPORT Approved for Public Release: Unlimited distribution
AMPC-033-038	5. MONITORING ORGANIZATION REPORT NUMBER(S) AFOSR-TR- 89-0840

6a. NAME OF PERFORMING ORGANIZATION Applied Microwave Plasma Concepts, Inc.	6b. OFFICE SYMBOL (If applicable) AMPC	7a. NAME OF MONITORING ORGANIZATION Air Force Office of Scientific Research/NP	
6c. ADDRESS (City, State, and ZIP Code) 2075-N Corte Del Nogal Carlsbad, CA 92009		7b. ADDRESS (City, State, and ZIP Code) Bolling Air Force Base, Bldg 410 Washington, DC 20332-6448	
8a. NAME OF FUNDING/SPONSORING ORGANIZATION Air Force Office Of Scientific Research/NP	8b. OFFICE SYMBOL (If applicable) AFOSR	9 PROCUREMENT INSTRUMENT IDENTIFICATION NUMBER F49620-88-C-0101	
8c. ADDRESS (City, State, and ZIP Code) Bolling Air Force Base, Bldg 410 Washington, DC 20332-6448		10 SOURCE OF FUNDING NUMBERS	
		PROGRAM ELEMENT NO. 61102F	PROJECT NO. 2301
		TASK NO A8	WORK UNIT ACCESSION NO

11. TITLE (Include Security Classification)
A Two-Stream Plasma Electron Microwave Source for High-Power Millimeter Wave Generation (U)

12. PERSONAL AUTHOR(S)
Gareth E. Guest and Raphael A. Dandl

13a. TYPE OF REPORT Final	13b. TIME COVERED FROM 88/08/01 TO 89/01/31	14. DATE OF REPORT (Year, Month, Day) 89/03/29	15 PAGE COUNT 61

16. SUPPLEMENTARY NOTATION

17. COSATI CODES			18. SUBJECT TERMS (Continue on reverse if necessary and identify by block number)
FIELD	GROUP	SUB-GROUP	

DTIC ELECTE JUL 3 1989 S A D

19. ABSTRACT (Continue on reverse if necessary and identify by block number)

A novel high power millimeter/microwave source is proposed in which one or more pairs of interpenetrating streams of electrons, flowing through a background plasma in a static magnetic field are used to generate a hot-electron plasma that is confined in a mirror-like magnetic field. Energy stored in the anisotropic, hot-electron plasma is then used to amplify pulses of unstable plasma waves to large amplitude by selective deactivation of mechanisms that stabilize the hot-electron plasma during the energy accumulation phase when the density of hot electrons is rapidly increased through the beam-plasma interaction. The Phase I program has yielded a design for an experimental arrangement capable of verifying the key aspects of this novel source concept, as well as a theoretical framework for interpreting the empirical Phase II results produced by the experimental device and extrapolating those results to evaluate the suitability of the proposed source to meet the requirements of various high power microwave and millimeter wave defense and industrial applications. The experiments will be carried out in a timely and cost-effective way by employing the AMPHED experimental facility at AMPC.

20. DISTRIBUTION/AVAILABILITY OF ABSTRACT ☒ UNCLASSIFIED/UNLIMITED ☐ SAME AS RPT. ☐ DTIC USERS	21. ABSTRACT SECURITY CLASSIFICATION Unclassified
22a. NAME OF RESPONSIBLE INDIVIDUAL Dr. Robert J. Barker/NP	22b. TELEPHONE (Include Area Code) (202)767-5011
	22c. OFFICE SYMBOL AFOSR/NP

DD FORM 1473, 84 MAR 83 APR edition may be used until exhausted. All other editions are obsolete

SECURITY CLASSIFICATION OF THIS PAGE
Unclassified

89 6 29 026

A TWO-STREAM PLASMA ELECTRON MICROWAVE SOURCE FOR HIGH-POWER MILLIMETER WAVE GENERATION

Small Business Innovation Research (SBIR) Program
Phase I

FINAL REPORT

by

G.E. Guest and R.A. Dandl

AMPC, Inc.

March 29, 1989

Work supported by
Air Force Office of Scientific Research
Contract No.
F49620-88-C-0101

NOTICES

"The views and conclusions contained in this document are those of the authors and should not be interpreted as necessarily representing the official policies or endorsements, either expressed or implied, of the Air Force Office of Scientific Research or the U.S. Government."

This report was prepared as an account of work sponsored by the United States Government. Neither the United States nor the Department of Defense, nor any of their employees, nor any of their contractors, subcontractors, or their employees, makes any warranty, expressed or implied, or assumes any legal liability or responsibility for the accuracy, completeness or usefulness of any information, apparatus, product or process disclosed, or represents that its use would not infringe privately owned rights.

TABLE OF CONTENTS

1. INTRODUCTION

A growing number of defense applications of microwave and millimeter wave radiation present requirements that cannot be satisfactorily met with existing fundamental mode sources. These requirements include high power at high frequency with high efficiency, longer pulse lengths, tunability, and amplifier operation together with compact size, ruggedness and good reliability. An illustrative example in electronic warfare is the destruction of electronic controls, sensors, and communication systems. There the most effective approach to coupling microwave power into the target utilizes super-power pulses with rapid rise times at the characteristic operating frequency of the target system. These frequencies are already high and expected to be higher in next-generation systems. Even now, high power is available only at frequencies below the characteristic frequencies of offensive weapons systems; and coupling must therefore be primarily through apertures not intended for microwave propagation with far lower efficiency than would be possible for direct coupling.

The capabilities of existing sources for meeting these requirements are limited largely because the generation of power is based on the passage of high-energy electron beams through resonant structures. The maximum power emitted by such devices decreases rapidly with increasing frequency, $Pf^2 \sim$ constant, where P is the power emitted at frequency f. This limitation arises principally because the size of the resonant structure is proportional to the wavelength, $\lambda = c/f$; and increasing the frequency (decreasing the wavelength) increases the power density that must be handled by the resonant structure. The resulting power density limitation in conventional microwave sources is further exacerbated at high power by the need to increase the electron beam voltage to reduce space-charge effects which would otherwise degrade the source performance.

The microwave source concept proposed here circumvents the conventional beam transit time, resonant structure, and space charge limitations by storing energy in a magnetic-mirror confined, electrically neutral, hot-electron plasma and periodically transforming a fraction of this stored energy into pulses of very high peak power. The transformation is mediated by a whistler wave launched at one end of the mirror-confined plasma, propagating along the magnetic lines of force, amplified by the anisotropic hot-electron plasma, and subsequently collected and focused by quasi-optical elements at the opposite end of the plasma. The operating frequency of this amplifier is determined by the strength of the static magnetic field and can therefore be scaled to very high values. The gain is determined by the physical dimensions and the energy density of the mirror-confined plasma so that the output power can be increased by scaling in size. Because both the operating frequency and the plasma energy density increase with increasing magnetic field strength, it appears that the peak power achieved in the proposed concept will increase with frequency (as well as the volume of the magnetic mirror) to give highly favorable scaling properties for defense applications. The resulting source can operate in amplifier or oscillator modes, can have high efficiency and be implemented in a rugged, compact embodiment.

The mirror-confined, hot-electron plasma that comprises the active medium responsible for amplification of the incident whistler results from the collective interaction of two or more oppositely directed electron streams with a mirror-confined background plasma. Experimental and theoretical studies of hot-electron plasmas created by beam-plasma interactions confirm the presence in the plasma of many separate regions of high field strength which are individually coherent but mutually incoherent. Such a volume distribution of independent regions is not suitable for the direct generation of useful microwave power; but it is extremely efficient

for stochastic heating of a minority of the plasma electrons to create a mirror-confined hot-electron plasma. The energy stored in this plasma can, in turn, be used either to amplify incident whistler waves propagating along the lines of force or as the source of spontaneous oscillations of whistler wave power. In effect, energy is stored throughout the plasma volume by the beam-plasma interaction but transformed into a coherent, two-dimensional form by the unstable whistler wave.

To recapitulate, the high-power microwave source concept to be developed in this project circumvents many of the limitations inherent in conventional microwave sources:

1) Limitations arising from the finite transit time of beam electrons through the resonant structure are circumvented by using the energy stored in a relativistic-electron plasma that is confined in a magnetic-mirror trap.
2) Space-charge limits on the beam are removed, since the relativistic electron plasma is electrically neutral.
3) The need for a metallic slow wave structure is obviated by having the stored energy transformed into microwave fields through the amplification of whistler waves that are guided by the magnetic field and the plasma.
4) The technology for storing energy in the hot-electron plasma uses simple steady-state streams of electrons flowing along the magnetic lines of force through a background plasma, and can be implemented in a rugged, compact embodiment.
5) The operating frequency of the source is determined by the strength of the static magnetic field, and can therefore readily be tuned as well as scaled to high values.
6) The gain and maximum output power are determined by the physical dimensions and the energy density of the mirror-confined

hot-electron plasma, so that output power can be increased by scaling in size, and external magnetic field strength.

Results achieved in Phase I of this project and summarized in Section 3.1 confirm the feasibility of accumulating significant quantities of kinetic energy in a mirror-confined hot-electron plasma using simple interpenetrating streams of electrons in a background plasma, as indicated schematically in Figure 1. Under suitable operating conditions, electrostatic waves propagating nearly parallel to the magnetic lines of force are driven to large amplitude by the collective interaction of the electron streams with the cold, background plasma. (1) Nonlinear processes are known to couple the large amplitude electrostatic waves to electromagnetic waves at twice the local upper hybrid frequency. (2) These waves propagate outward into regions where they can be preferentially absorbed by the energetic, mirror-confined electrons through cyclotron damping at overtones of the relativistic electron gyrofrequency. (3) If the plasma is enclosed in a suitable conducting shell, the electromagnetic waves can be confined in the plasma region and absorbed by the hot-electron plasma in ways that are fundamentally identical to the processes responsible for hot electron generation in microwave heated plasmas. Other electrostatic waves propagating at oblique angles to the magnetic field can also be driven to large amplitude by the beam-plasma interaction. These waves extract parallel kinetic energy from the electron streams and increase their perpendicular kinetic energies. As a result, some of the energetic-beam electrons are trapped in the magnetic mirror.

The mirror-confined hot-electron plasma resulting from the beam-plasma interaction forms an active medium that can be used to amplify incident whistler waves and thereby transform the kinetic energy of the hot-electron plasma into microwave field energy. An indication of the plasma conditions under which high-gain amplification of whistlers can

occur is shown in Figure 2, where the threshold for growth is plotted as a function of the hot-electron temperature anisotropy and relative energy density (4), as discussed at length in Section 3.3. For efficient operation of this concept it is necessary to accumulate the hot-electron plasma under stable conditions, and then rapidly alter the plasma state so that whistler amplification is possible. This rapid alteration in the plasma conditions can be accomplished in principle through adiabatic magnetic compression, reduction of the cold-plasma density, or a combination of the two. Adiabatic magnetic compression appears to be particularly well suited to amplifier operation, while supplemental electron cyclotron heating for control of the hot-electron temperature anisotropy and the cold-plasma density, together with the use of quasi-optical resonator techniques, is especially attractive for operation in the pulsed oscillator mode. Both the oscillator and amplifier modes are expected to yield high-power pulses of coherent radiation. (5)

1.1 Identification of the Key Issues

Earlier work (1) on the formation of hot-electron plasmas by beam-plasma interactions has not included an adequate characterization of the equilibrium properties of the hot-electron component. In order to utilize these hot-electron plasmas to amplify whistler waves it is necessary to characterize and control the spatial distribution of hot-electrons as well as their temperature anisotropy and relative energy density. Techniques for determining the most important hot-electron plasma parameters have been developed in connection with electron cyclotron heating research; (6) and these techniques can be applied to the hot-electron plasma generated by the beam-plasma interactions.

The optimization of beam-plasma generated hot-electron plasmas for the PEMS application can best be determined through an experimental demonstration of whistler wave gain, for operation in the amplifier mode, or

triggered high-power microwave pulses, for operation in the oscillator mode.

With regard to hot-electron plasma formation and whistler amplification, a valid theoretical model is needed to facilitate interpretation of experiments and optimization of the concept as well as scaling the results of Phase II experiments to Phase III conceptual devices.

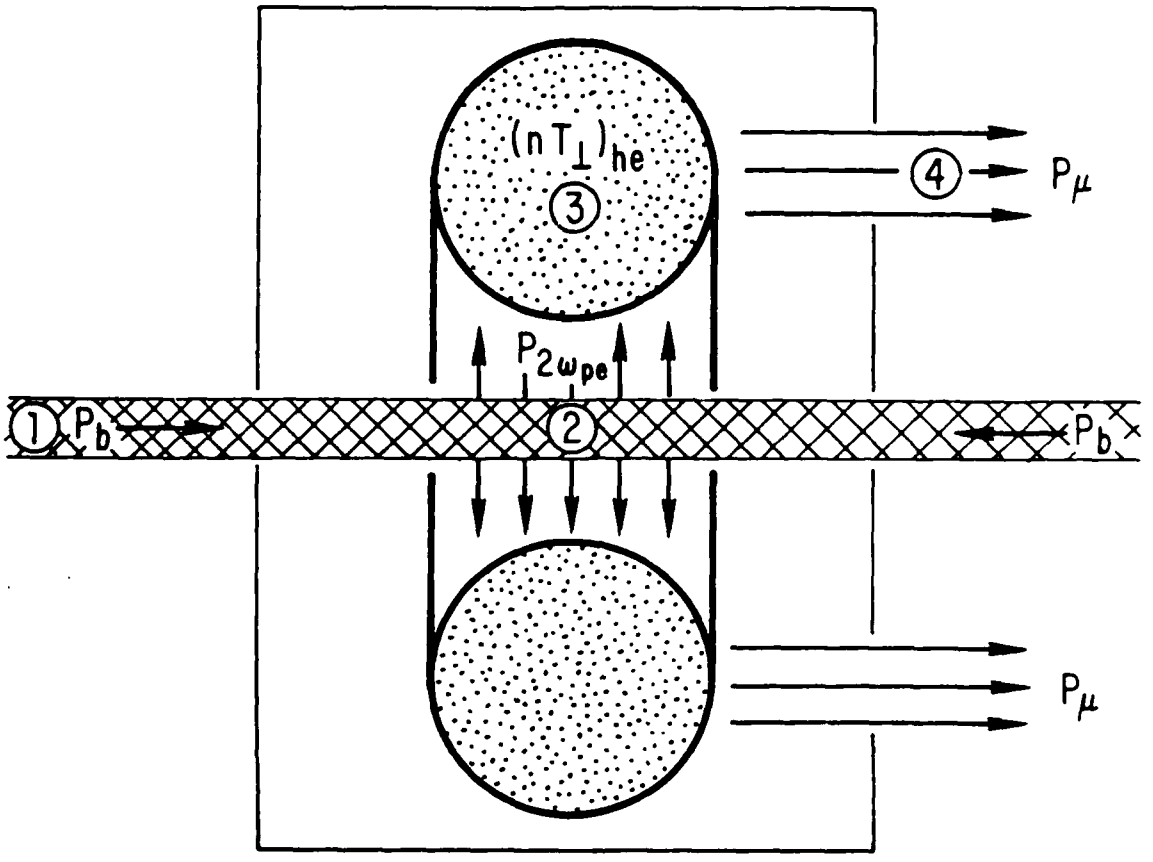

(1) DC Power input via steady-state electron beams

(2) Electromagnetic power at $2\omega_{pe}$ [$\sim 2\Omega_{he}$] generated by beam-plasma interactions

(3) Power generated by beam-plasma interactions stored in anisotropic, mirror-confined, hot-electron plasma

(4) Coherent, pulsed, high-power microwave output from unstable whistler waves

FIGURE 1a: Schematic representation of the Two-Stream PEMS Concept

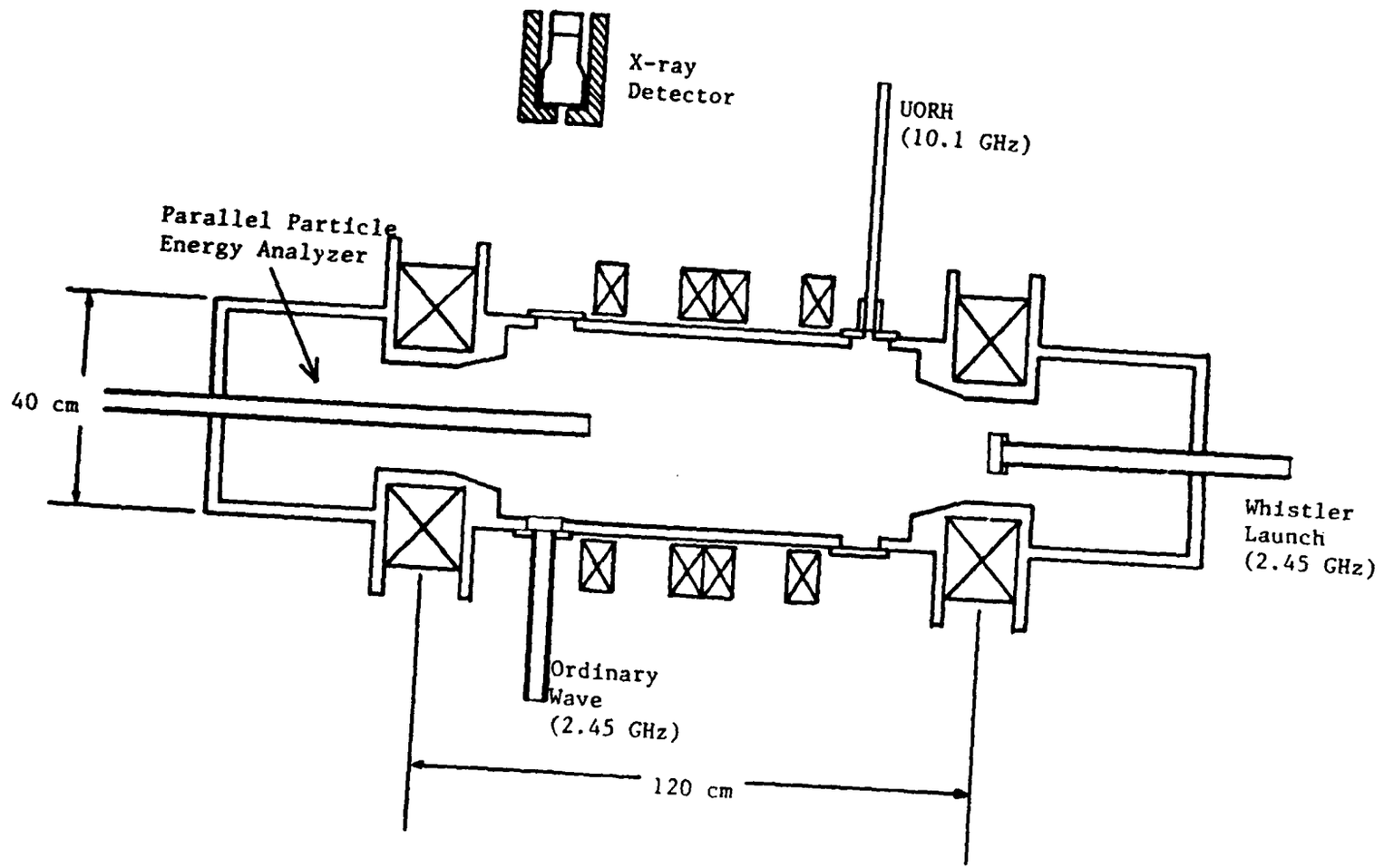

FIGURE 1b: Initial implementation of the Two-Stream PEMS concept in the AMPHED experimental facility.

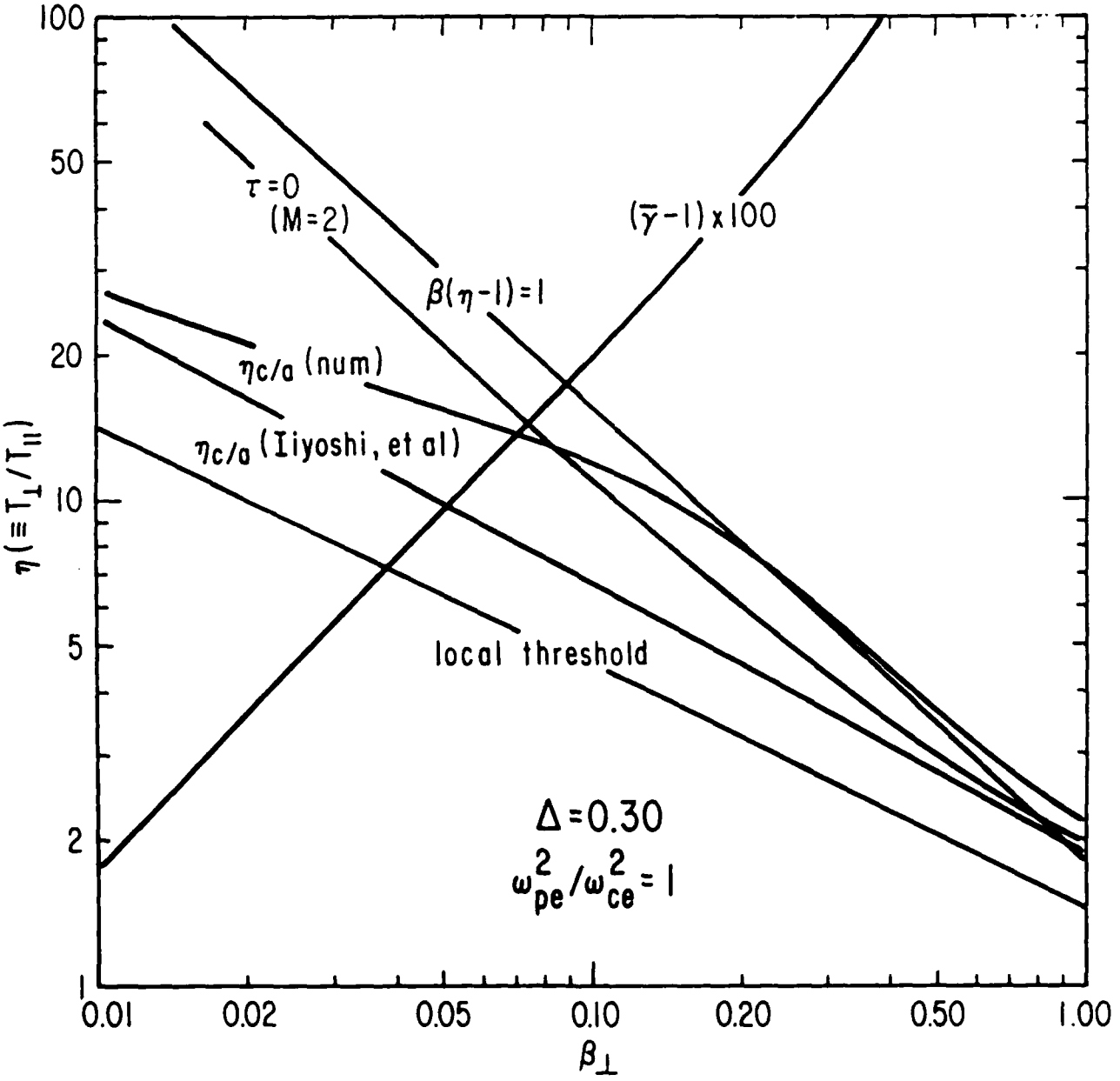

FIGURE 2: Predicted threshold conditions for convective and absolute growth of whistler waves in spatially inhomogeneous, anisotropic, finite-beta hot-electron plasmas.

2. TECHNICAL APPROACH

2.1 Technical Objectives

In order to demonstrate experimentally the potential advantages of the Two-Stream PEMS concept enumerated in the preceeding section, we have developed an experimental approach that can be implemented in a timely and cost-effective way using the existing AMPHED facility at AMPC, described in Section 3.2. This approach seeks to achieve three major objectives:

1) an experimental demonstration and characterization of efficient energy accumulation using the two-stream beam-plasma interaction in suitable conducting cavities;

2) the experimental demonstration of whistler amplification by the mirror-confined hot-electron plasma and/or triggered, high-power pulses in the oscillator mode of operation; and

3) the development of theoretical models to interpret the experimental results and evaluate the performance of conceptual systems using the Two-Stream PEMS approach.

These objectives can be accomplished through an experimental program that utilizes the existing AMPHED experimental facility together with a closely coupled theoretical effort aimed at developing a valid theoretical model of the experimental results. In this section we describe in some detail the technical approach to be used in this project.

2.2 Modification of the AMPHED Facility

The existing AMPHED experimental facility requires only minor modifications to permit the experimental production and characterization of hot-electron plasma generated by beam-plasma interactions. A symmetrical structure to generate two oppositely directed electron streams will be located in AMPHED as shown in Figure 1b. The streams will initially be powered by an existing 10 kV, 500mA power supply. The flat-field magnetic configuration in AMPHED provides a uniform interaction region up to 80 cm long. This large region of uniform magnetic intensity can be used to ensure strong growth of unstable electrostatic waves. The background plasma can be generated spontaneously by beam ionization of the ambient gas, in which case the major control of background plasma density is through control of the ambient gas pressure. In addition, since AMPHED is supplied with several sources of microwave power suitable for creation and control of the background plasma density and temperature, these can be used to achieve an unusual degree of control over these parameters for studies aimed at optimum generation of PEMS-relevant hot-electron plasmas.

Control of the background plasma density is expected to be particularly important in optimizing hot-electron production, since the electromagnetic power generated by the non-linear electrostatic waves is mainly at frequencies near twice the local upper hybrid frequency. We anticipate the most efficient generation of hot electrons if this power is near the second harmonic of the relativistic electron gyrofrequency in the region where hot electrons accumulate. Control of the background plasma density will allow us to vary the upper hybrid frequency to test this hypothesis.

The DC electrical supply for the AMPHED magnetic coils has recently been upgraded to provide the level of control required for precise determination of the diamagnetic fields created by hot-electron plasmas using arrays of Hall probes. (6) The spatial dependence of the hot-electron

energy density will be measured experimentally with these Hall probe arrays as well as by the traditional skimmer probes used successfully to characterize high energy density hot-electron plasmas in ELMO. (3) The local distribution of hot electrons in energy will be measured using x-ray techniques as in numerous earlier ECH hot-electron experiments. Background plasma parameters will be determined with conventional Langmuir probes presently in use on AMPHED.

2.3 Experimental Characterization of Hot-Electron Plasma Generation Using Beam-Plasma Processes

Following the installation of the beam-forming structure we anticipate an initial series of experiments aimed at optimizing the beam-plasma generation of hot-electron plasmas and establishing the operating conditions for which satisfactory hot-electron production is achieved. The system parameters expected to be particularly important to hot-electron production are the electron beam energy and density, the background plasma density, and the spatial extent and uniformity of the two-stream interaction region. We will optimize the hot-electron diamagnetic energy density with respect to these control parameters and seek to determine preliminary scaling relations that can be used to extrapolate the Phase II results for conceptualization of Phase III applications.

In order to facilitate the development of valid theoretical models of the hot-electron plasma formation, we will monitor the power spectrum of the electromagnetic radiation generated by the large amplitude electrostatic waves driven by the beam-plasma interaction. In this way we will seek to estimate the overall efficiency of the process as well as determine ways of enhancing that efficiency.

Having delineated a satisfactory range of operating conditions for generating hot-electron plasmas, we will undertake a more detailed characterization of these hot-electron plasmas. This characterization will include the spatial properties of the hot-electron component as well as the local distribution of hot electrons in energy. Conversion of the hot-electron energy into microwave power depends on the hot-electron temperature anisotropy and relative energy density. We will seek to identify the dependence of these properties on the externally controlled operating parameters such as ambient gas pressure and electron stream power, as well as supplemental ECH and/or UORH power.

2.4 Measurements of Whistler Amplification

At the present time AMPC is developing experimental techniques to measure the propagation and growth of whistler waves launched along magnetic lines of force and passing through magnetic-mirror confined plasmas. Whistlers are launched from a dielectric-loaded wave guide structure whose radiation pattern is modified by a shaped dielectric insert, as described in Section 3.2. Wavelengths of the propagating whistler are measured by microwave interferometric techniques, and local intensities are determined by RF probes as described in Section 3.2. In the second phase of the experimental program proposed here, we will utilize similar techniques to help characterize the amplification of whistlers by the hot-electron plasmas generated through the beam-plasma interactions. The amplified whistler will be detected and its power level determined using an array of horns mounted on the end opposite the launch structure.

2.5 Development of Valid Theoretical Models

In order to interpret the experimental results to be obtained in Phase II as well as to evaluate conceptual systems to be considered in Phase III, AMPC will develop and validate a theoretical model that encompasses the two major aspects of the Two-Stream PEMS concept; namely,

1) Efficient Formation of Mirror-Confined Hot-Electron Plasmas by Beam-Plasma Processes; and
2) Transformation of Plasma Energy to Coherent Microwave Power Through Whistler Amplification.

Within the first category we will seek to model the dominant electrostatic beam-plasma interactions, the processes that saturate the growth of the electrostatic waves, the three-wave processes governing the generation of electromagnetic waves, and the preferential absorption of these waves by mirror-confined hot electrons. The basic linear dispersion relation code describing growth of electrostatic beam-plasma modes has been used extensively in Phase I, as described in Section 3.1. The theory of the three-wave coupling has been developed by several authors (2) and can be validated using Phase II experiments. The preferential absorption of high-frequency electromagnetic waves by mirror-confined hot electrons has been studied experimentally and theoretically by AMPC scientists in the past few years. (3) These three separate components will be linked together to form the principal framework for the first major aspect of the Phase II modelling program.

The second major aspect will build on the earlier work done at AMPC to evaluate realistic threshold conditions and maximum amplification rates for whistler waves propagating through anisotropic, mirror-confined, hot-electron plasmas. (4) New theoretical studies will be undertaken to clarify the roles of relevant non-linear mechanisms controlling the onset of whistler growth, such as the relative cold-plasma density and temperature.

The mechanisms responsible for saturating the growth of whistlers will also be investigated in order to estimate the maximum output power in the amplifier mode.

2.6 Summary of the Phase I Technical Objectives

The main objective of the Phase I program was a preliminary design of an experimental device capable of demonstrating the validity of the basic elements of the concept:

1. Effective accumulation of significant levels of energy density in a mirror-confined, hot-electron plasma using interpenetrating electron streams in a background plasma; and

2. Amplification of externally launched whistler waves propagating along magnetic lines of force through the mirror-confined hot-electron plasma.

In order to accomplish this design objective, it was necessary to address a number of fundamental issues whose clarification provided a solid theoretical framework for the proposed concept. Among the most immediate issues were the following:

1. Optimal Conditions for Creating the Hot-Electron Plasma

A large empirical base of information, together with a body of somewhat idealized theory presently exists regarding the use of beam-plasma interactions to create mirror-confined hot-electron plasmas. This material was updated using relevant results from experiments and Fokker-Planck models of the electron cyclotron heating (ECH) process which

clearly establish the role of O-mode fields at overtones of the hot-electron gyrofrequency in forming high-beta, hot-electron plasmas. In this way, we sought to determine the available range of operating parameters and the sensitivity of the electron heating process to the major device parameters entering the design.

2. Alternative Ways of Controlling the Release of Stored Energy for High-Gain Amplification.

Two general approaches to bringing the plasma rapidly to the threshold for whistler amplification are presently identified; namely, control of the hot-electron temperature anisotropy and the magnetic field uniformity, and control of the background cold-plasma density and temperature. A more detailed analysis of each approach is needed to implement one or both of these approaches in the device design.

3. Quasi-Optical Output Coupling Structures

An analysis of the propagation, growth and/or damping of whistler waves in candidate device concepts is needed to support the design of effective coupling structures to guide the amplified whistler wave into suitable microwave transmission systems.

3. MAJOR RESULTS ACCOMPLISHED

3.1 Creation of Hot-Electron Plasmas Using Beam-Plasma Interactions

In Phase I of this project we have investigated the fundamental processes expected to play dominant roles in determining the efficiency with which beam-plasma interactions will generate a substantial density of relativistic, mirror-confined electrons. These include three major phenomena:

1) the growth of unstable electrostatic waves driven by the two streams of electrons interacting with the background plasma;
2) the non-linear coupling of oppositely-directed pairs of large-amplitude electrostatic waves to excite an electromagnetic wave propagating radially outward; and
3) the preferential absorption of this electromagnetic wave by energetic electrons confined in a magnetic mirror.

Each of these three separate phenomena has a substantial empirical and theoretical base which we will briefly review here. Their integration to form an efficient technique for accumulating energy in a mirror-confined hot-electron plasma is a major objective of Phase II of the present project. It will be clear from the review of each separate phenomenon that the overall feasibility of the concept is strongly supported and the prognosis for efficient energy storage by the proposed technique is excellent.

3.1.1 Unstable Electrostatic Waves in the Proposed Configuration

The proposed proof-of-principle plasma configuration consists of two co-linear interpenetrating, oppositely-directed electron streams flowing along the axis of the external magnetic-coil system through a low-temperature background plasma. The properties of unstable electrostatic waves in this configuration have been studied extensively both experimentally (1) and theoretically. (7) The most rudimentary theoretical model capable of describing the propagation and growth of electrostatic waves in this configuration consists of infinite, homogeneous plasma components in a uniform steady magnetic field. The dispersion relation for electrostatic waves in such a plasma was derived by Harris (8). In the limit of negligible thermal speeds, this dispersion relation was shown to correspond well with laboratory experiments (1). Here we summarize the main predictions of the theoretical model bearing on the excitiation of large amplitude electrostatic waves that can interact non-linearly to excite electromagnetic waves suitable for generating a mirror-confined hot-electron plasma.

The dominant mode of instability arises from interactions between each separate beam and the background plasma. The properties of the dominant mode are thus identical to those of the single-beam cold-plasma system studied by O'Neil et. al. (9) The frequency of the fastest growing mode is very close to the electron plasma frequency, as shown in Fig. 3. Here we display the wave vector, the real frequency, and the growth rate of the fastest growing mode for a range of background electron plasma frequencies with the beam density fixed. The wave vector has been chosen to maximize the growth rates. Each of the parameters is normalized as follows:

1) the wave vector is expressed through the dimensionless quantity $H \equiv k_{||} v_b / \Omega$, where $k_{||}$ is the component of the wave vector

parallel to the static magnetic field, v_b is the beam speed, and Ω is the electron gyrofrequency;

2) the wave frequency and growth rate are normalized by the electron gyrofrequency, $W = \omega/\Omega$.

3) the background electron plasma frequency is normalized by the electron gyrofrequency, $W_e = \omega_{pe}/\Omega$, where $\omega_{pe}^2 = e^2 n_e/m\epsilon_o$. The electron charge and mass are $-e$ and m, the background electron density is n_e, and ϵ_o is the permittivity of free space;

4] the electron beam density, n_b, is expressed through the equivalent plasma frequency, $W_b \equiv \omega_{pb}/\Omega$, with $\omega_{pb}^2 = e^2 n_b/m\epsilon_o$.

As is clear from Figure 3, the fastest growing mode satisfies two approximate criteria; namely,

$$W \simeq W_e \text{ or } \omega \simeq \omega_{pe}$$

and

$$H \simeq W_e \text{ or } kv_b \simeq \omega_{pe}.$$

The maximum growth rate is given roughly by

$$W_i \sim 0.6[W_b^2 W_e]^{1/3},$$

where W_i is the imaginary part of the frequency, γ, normalized by the electron gyrofrequency. Thus,

$$\gamma \simeq 0.6(n_b/n_e)^{1/3}\omega_{pe}.$$

Note that the coefficient 0.6 is close to the corresponding analytic estimate $[3^{1/2}/2^{4/3}] = 0.687$ deduced by O'Neil et. al. (9) The dependence of the growth

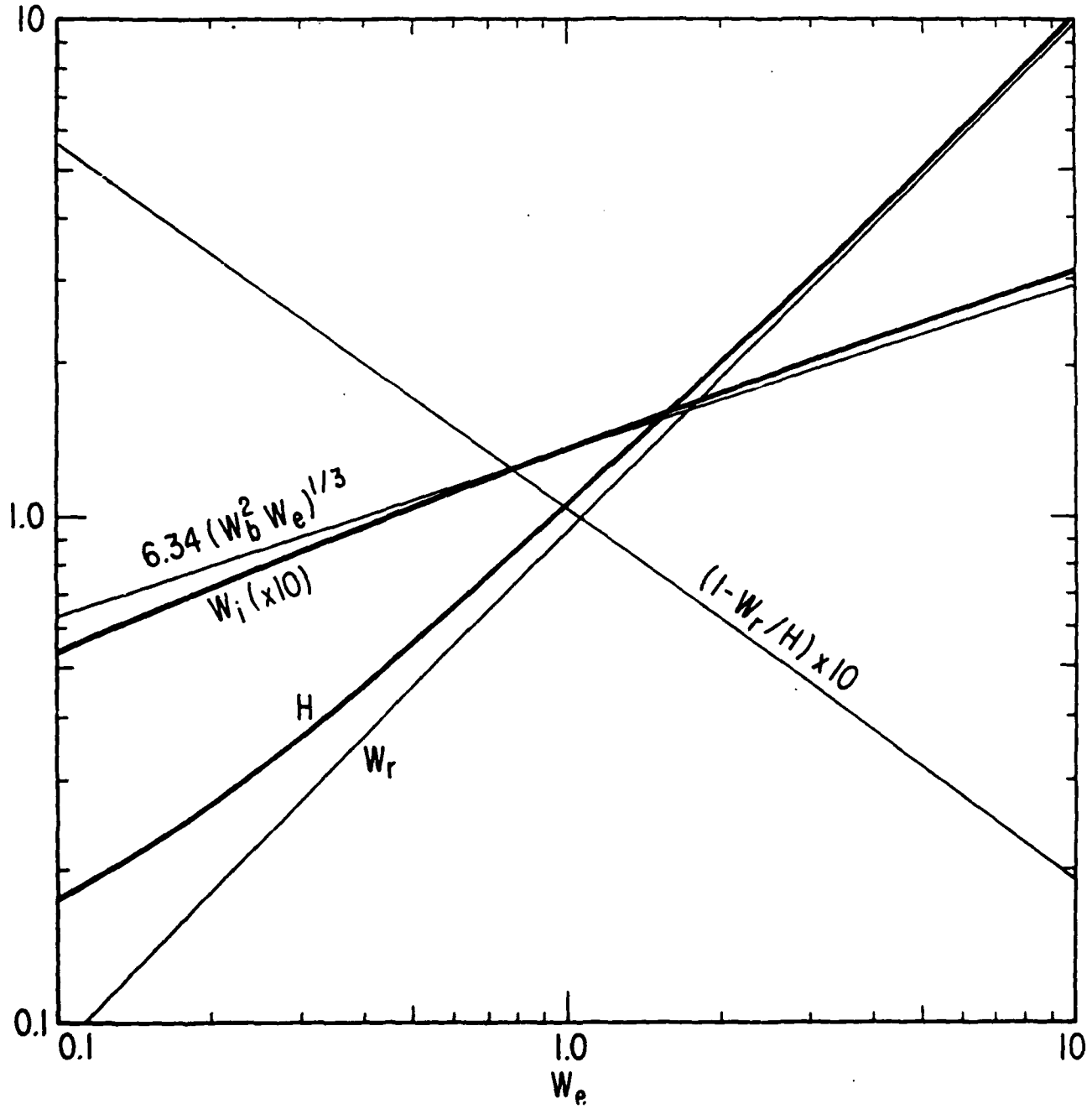

FIGURE 3: Properties of the fastest growing electrostatic beam-plasma instability: the (parallel) wave vector $H = k_{||} v_b/\Omega$; the real frequency, $W_r = \omega/\Omega$; and the growth rate, $W_i = \gamma/\Omega$, where Ω is the electron gyrofreuqency. The background electron plasma frequency is $W_{pe} = \omega_{pe}/\Omega$

rate on the electron-stream density is shown in Fig. 4, where W_i is displayed as a function of W_b for $W_e = 1$ and $H = 1.04$, the value for maximum growth rate.

In obtaining the results shown in Figs. 3 and 4 we have chosen the wave vector to be parallel to the magnetic field; i.e., $k_\perp \propto 0$. For electron streams of finite radial extent the boundary conditions at the surface of the stream may require a finite value of $k_\perp$. For example, a suitable boundary condition for many cylindrical systems is $J_0(k_\perp a) = 0$, where J_0 is the Bessel funcion of order zero, and a is the radius of the column. For such a case, $k_\perp \propto 2.4/a$. To illustrate how oblique propagation affects the growth rate of the modes shown in Fig. 3 and 4, we display in Fig. 5 a plot of $W_i(\theta)$, where $\theta = \tan^{-1}(k_\perp/k_\parallel)$. For the particular case chosen here, $W_e = 1$, $W_b = 0.1$ and $H = 1.04$, 0.8, and 0.6. The growth rate is substantially reduced for $\theta \neq 0$; but γ vanishes only for propagation nearly perpendicular to the magnetic field. It is clear from Fig. 5, however, that the obliquely propagating wave is entirely distinct from the wave that propagates parallel to the magnetic field. Indeed, the growth rate is maximized for non-zero angles of propagation for $H = 0.8$ and 0.6; whereas the maximum growth rate occurs for $\theta = 0$ and $H = 1.04$.

The sub-dominant obliquely-propagating mode arises from an interaction between the two counter-streaming electron beams, in which a longitudinal space-charge wave on one stream couples to a cyclotron wave on the opposite stream. A particularly noteworthy feature of this mode is that it transfers parallel momentum from each stream into perpendicular momentum of the oppositely-directed stream. Excitation of this mode could significantly enhance the magnetic trapping of energetic-beam electrons collectively scattered out of the streams.

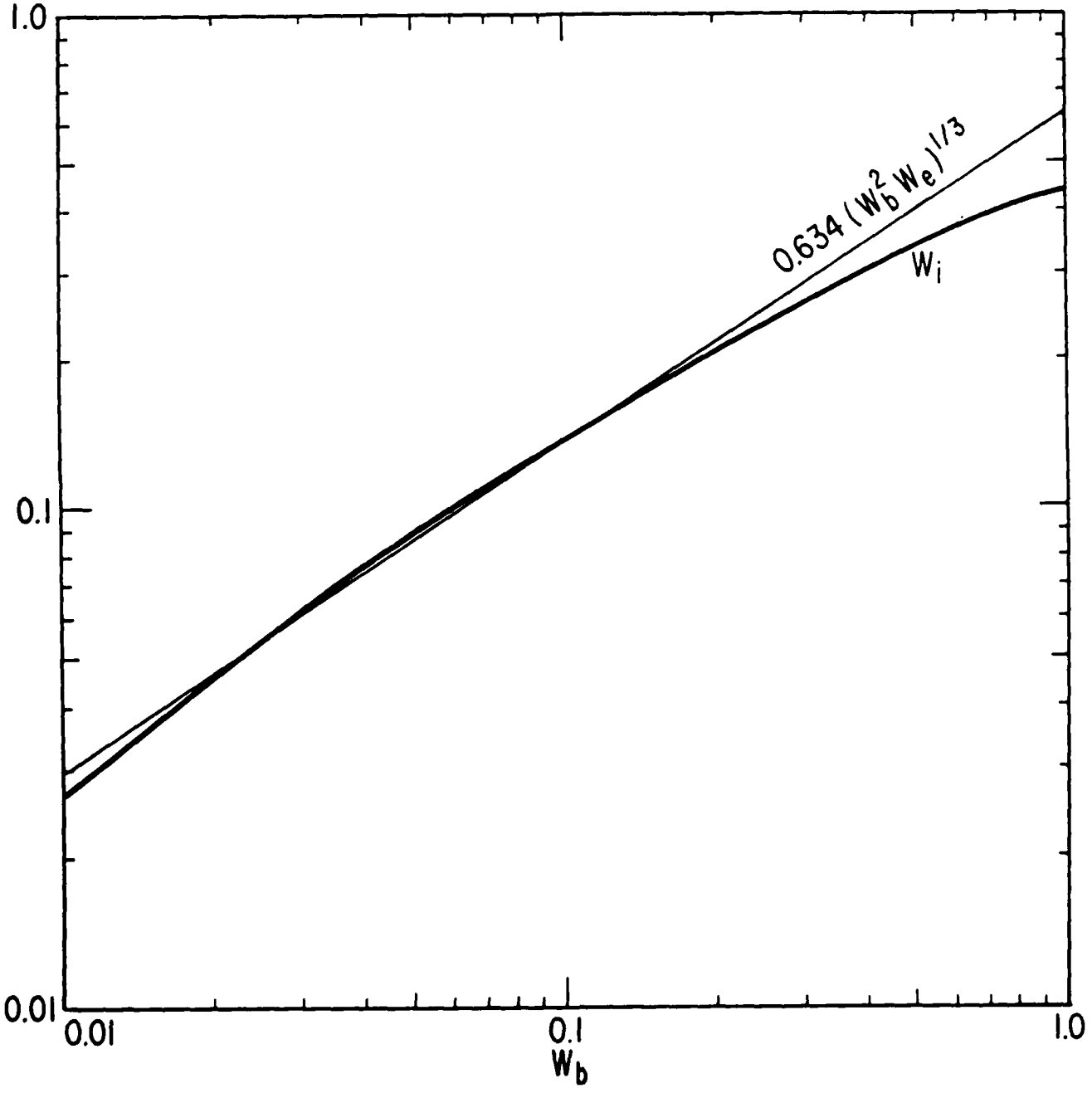

FIGURE 4: Dependence of growth rate on the electron beam density. $W_b = \omega_{pe}/\Omega$ is the electron plasma frequency corresponding to the beam density.

The electrostatic waves are predicted to grow at the linear growth rate until the associated electrostatic potential is large enough to trap the beam electrons (9) The growth then ceases at this level; namely,

$$e\phi_{sat} \propto m(v_b - \omega/k_{||})^2/2 = E_b(1 - W_r/H)^2,$$

where $E_b = mv_b^2/2$ is the kinetic energy of the beam electrons. The parallel phase velocity of the fastest growing wave is proportional to but slightly less than the beam velocity. In Fig. 6 we display $1 - W_r/H$ as well as other wave parameters versus $(n_b/n_e)^{1/3}$, from which we obtain

$$1 - W_r/H \propto 0.5(n_b/n_e)^{1/3},$$

in agreement with O'Neil et. al. (9) When the linear growth saturates, a fraction of the kinetic energy of the beam electrons is converted to electrostatic energy:

$$\varepsilon_o E_{es}^2/2 \propto n_b E_b (n_b/n_e)^{2/3}/4.$$

This process has been observed in numerous simulations of the beam-plasma interaction. (10)

O'Neil et. al. (9) show how the evolution of the fastest growing wave leads to a very narrow spectral distribution of the wave energy in wave number. The initial width, $\Delta k_{||}/k_{||} \sim (n_b/n_e)^{1/3}$, is predicted to be reduced to a much narrower range given by

$$\delta k/k_o = 3(\ln 2/N)^{1/2} 2^{-5/6} (n_b/n_e)^{1/3},$$

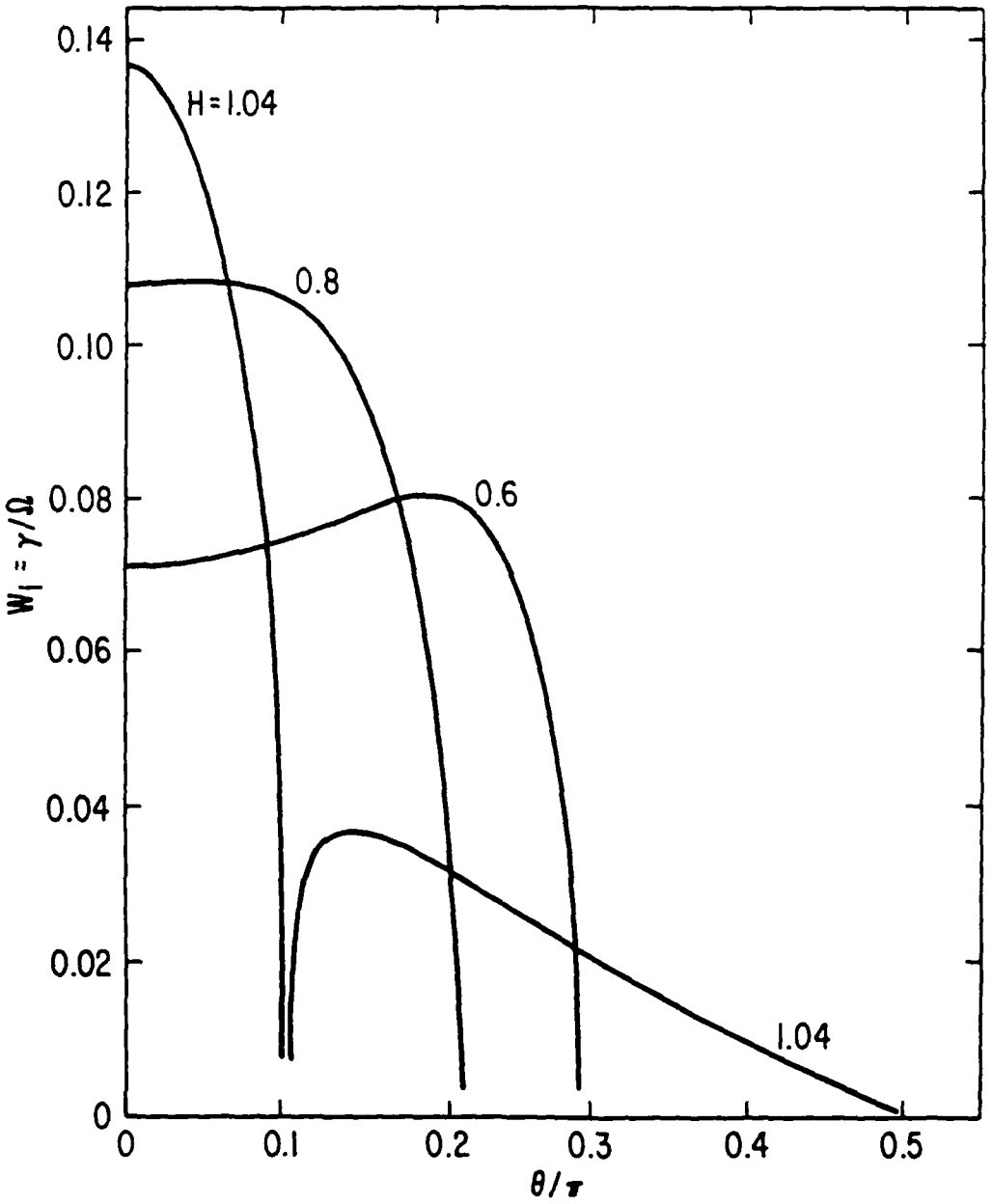

FIGURE 5: Dependence of growth rate on the angle of propagation relative to the direction of the magnetic field.

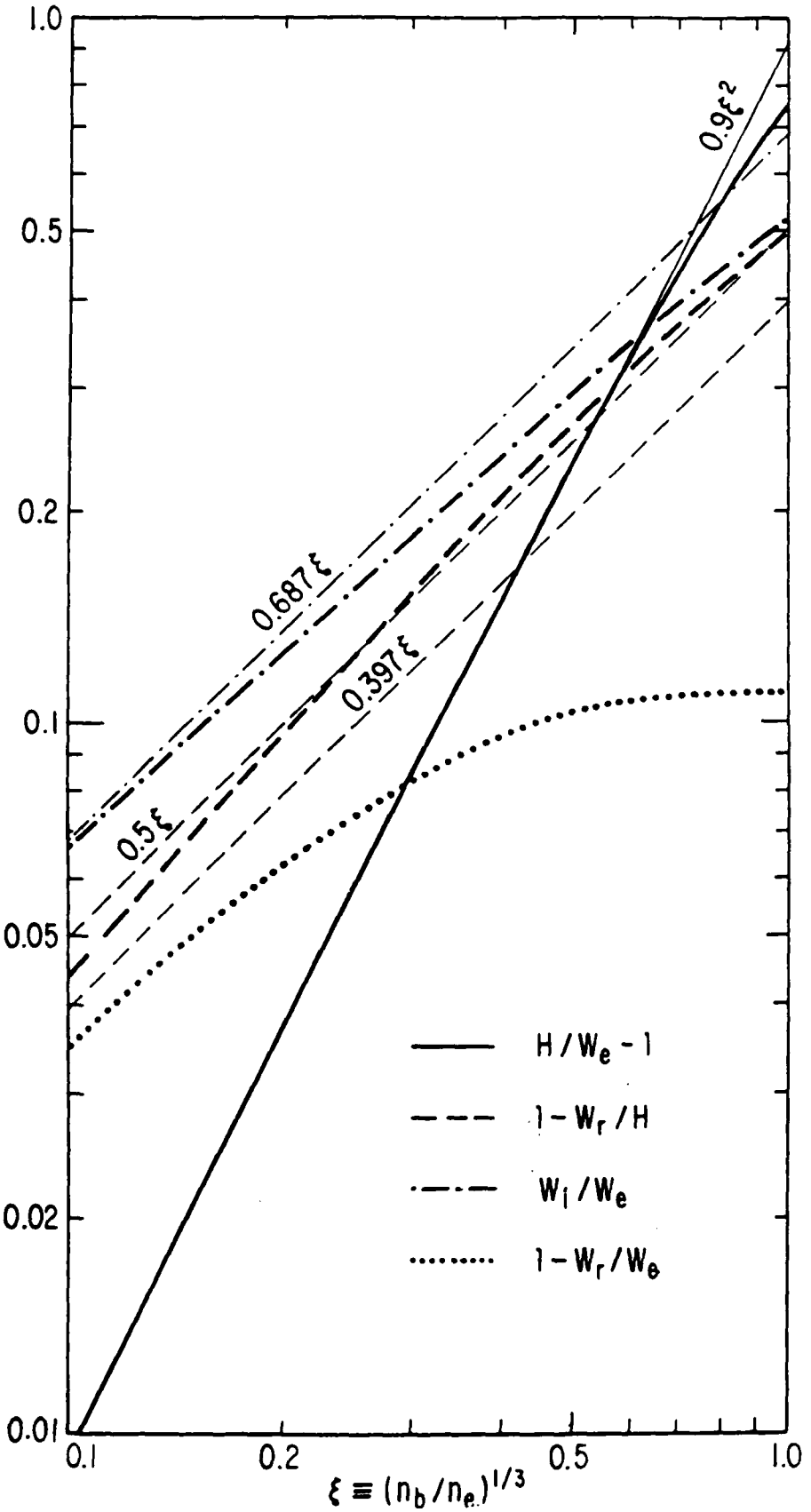

FIGURE 6: Dependence of properties of the fastest growing wave on the relative density of the beam electrons and the background plasma electrons, n_b/n_e. Here $\xi \equiv (n_b/n_e)^{1/3}$.

where N is the number of e-foldings in wave amplitude before saturation of the linear growth, $N = O[10^2]$. The spectral density of electrostatic field energy is predicted to increase roughly a factor of 7 - 10 through this narrowing of the spectral distribution. As O'Neil et. al. (9) observe, the saturated wave is essentially a pure sinusoidal disturbance.

3.1.2 The Non-Linear Three-Wave Interaction

The large amplitude electrostatic waves described in Sect. 3.1 are generated by each of the co-linear, oppositely-directed electron streams interacting with the background plasma. When pairs of these oppositely-directed electrostatic waves interact they can generate an electromagnetic wave propagating radially outward from the electron beam region. This fusion of two electrostatic waves ("plasmons") to form an electromagnetic wave ("photon") has been studied theoretically and experimentally for a number of years. (2) Here we briefly summarize the properties of this three-wave interaction as it applies to the Two-Stream PEMS concept. To recapitulate, it is this three-wave interaction by which some of the steady-state electron stream energy is converted to electromagnetic radiation at frequencies suitable for efficient generation of a mirror-confined hot-electron plasma. The DC power introduced through the electron streams is thus accumulated and stored in the anisotropic, hot-electon plasma in a form from which it can be efficiently transformed into coherent pulses of microwave radiation.

As was discussed extensively by Harris (11), it is useful to view the three-wave process from a quantum mechanical viewpoint. Each wave can then be assigned an energy, $\hbar\omega$, and momentum, $\hbar k$. Here $\hbar$ is Planck's constant divided by 2π. Conservation of energy and momentum in the three-wave interaction thus requires that

$$\omega_1 + \omega_2 = \omega_3 \quad \text{and} \quad \vec{k}_1 + \vec{k}_2 = \vec{k}_3.$$

We have designated the two electrostatic waves with subscripts 1 and 2, and the electromagnetic wave with subscript 3. As we have seen, the fastest growing electrostatic waves have frequencies very near the electron plasma frequency of the background plasma:

$$\omega_1 = \omega_2 \simeq \omega_{pe}.$$

The wave vectors of the electrostatic waves can be nearly equal in magnitude but with opposite sign, so that $k_3 << k_1 \simeq -k_2$. Thus, the electromagnetic wave can be emitted with vanishingly small values of $k_{||}$, and will propagate radially outward away from the spatial region occupied by the streams. Through the three-wave process the electron streams serve as a source of bursts of microwave radiation at frequencies near $2\omega_{pe}$.

The efficiency with which the DC electron stream energy is converted to electromagnetic power is still somewhat uncertain. Several different theoretical models have been used to estimate this conversion efficiency (12); but the experimental measurements show substantially higher efficiencies than predicted theoretically. (2) The predicted parametric dependence of the electromagnetic power emitted can be seen from the expression derived by Kaplan and Tsytovich (12):

$$\beta_\mu \propto [2.4\pi/\sqrt{3}](\omega_{pe}^2/n_0 mc^3) \int_{\sqrt{3}\,\omega_{pe}/c}^{k_D} dk\, (W_{es}\omega_{pe}/ck)^2$$

Here $\hat{P}_\mu$ is the power density of the electromagnetic wave, W_{es} is the saturated energy density of the electrostatic waves per unit interval of k, and the integral extends up to the Debye wave number, k_D.

Following O'Neil et. al. (9) we estimate

$$W_{es} \sim n_b E_b (n_b/n_e)^{2/3} / \delta k,$$

where

$$\delta k \sim k_o (n_b/n_e)^{1/3} N^{-1/2}.$$

A rough estimate of the integral can be obtained by assuming that W_{es} has its saturated value over the interval $[k_o - \delta k/2, k_o + \delta k/2]$ and is zero otherwise:

$$\hat{P}_\mu \sim 0.8\pi\sqrt{3}\,[\omega_{pe}^2/n_e mc^3]\, W_{es}^2 (v_b/c)^2 \delta k.$$

The microwave power density is thus predicted to vary roughly as

$$\omega_{pe}\, n_b E_b \sqrt{N}\, (E_b/mc^2)(n_b/n_e)^2\, (v_b/c)^3.$$

For typical anticipated system parameters the predicted power density is $O(1 W/cm^3)$.

3.2 EXPERIMENTAL ARRANGEMENT AND OPERATION OF THE AMPHED FACILITY

3.2.1 Description of the AMPHED facility

AMPHED is a flexible CW magnetic-mirror facility comprised of six field coils as shown schematically in Fig. 7. The plasma confinement region is enclosed in a cylindrical, microwave-tight, aluminum vacuum vessel with enough penetrations to accommodate multiple microwave power sources and plasma diagnostics.

The magnetic field configuration to be used in the experiments proposed here is produced by connecting the two center coils in parallel, and then in series with the other coils which are fed by a 200 kVA DC power supply. While the maximum overall mirror ratio is about 2, the mirror ratio at the cyclotron resonance interaction region can be varied from 1:1 to 2:1. The location of the ECR layer and the mirror ratio at this location for a given heating frequency can be controlled precisely by adjusting the D.C. magnetic coil current. This feature is particularly advantageous for investigation and optimization of electron cyclotron heating mechanisms which are predicted to depend strongly on the local magnetic field gradient at the location of resonance. (14)

A plot of the magnetic field configuration is shown in Fig. 8. (The magnetic field calculation has been verified to an accuracy of 0.5% by measuring the field profile along the mirror axis using an array of Hall probes.) There are two noteworthy features of this magnetic configuration:

1. The region of minimum field is nearly uniform throughout an axial length of 80 cm and a radial extent of 15 cm, a volume of 57 liters. The average scale length characterizing the variation of field strength within this region is greater than 100 cm.
2. Near the mirror throat the magnetic field strength increases to twice its midplane value within 20 cm.

The long axial dimension of the AMPHED facility also provides several other operational conveniences. For example, the magnetic field near one end of the mirror configuration can be reduced locally, yet the field topology and scale-length on the other end can be kept relatively unaltered. This modification causes the heated particle to gain additional parallel energy due to the conservation of their magnetic moment, thus allowing them to overcome the (usually) positive ambipolar potential well and to be collected by a parallel-energy particle analyzer, as described in detail in the following section.

At present microwave power is introduced in three different heating configurations, as also shown in Fig. 7. Whistler waves are launched from a 2.45 GHz, 800 watt, commercial microwave oven coupled into the high field mirror throat region using a dielectric-loaded C-band waveguide, terminated with a tapered Teflon slab. Ordinary waves, also at 2.45 GHz, are launched from a side port directly illuminating the flat-field region near the mirror minimum. The Teflon loaded waveguide is oriented in such a way that the E-plane of the waveguide is parallel to the magnetic field lines, i.e. $\vec{E} \parallel \vec{B}$, where $\vec{E}$ and $\vec{B}$ are the wave electric field and the vacuum magnetic field, respectively. The UORH power, transmitted from a 10.1 GHz, cw klystron amplifier, is coupled to the system through another side port. This power is near the 4th harmonic of the fundamental heating frequency of 2.45 GHz. A commercial 4-port hybrid coupler is used between the standard X-band wave guide and the aluminum vacuum vessel to improve the impedance matching with the plasma.

Plasmas are typically produced in argon, nitrogen or hydrogen gas at the operating pressure of 10^{-5} - 10^{-3} torr. Because significant plasma pumping generally occurs in this pressure range, the ionization gauge that monitors the operating pressure is located in the center region of the vacuum system

to obtain more meaningful pressure readings.

3.2.2 Diagnostics

The diagnostics to be used in this investigation are indicated in Fig. 7. The X-ray detector is a lead collimated commercial NaI(Tl) scintillation spectrometer and Pulse Height Analyzer to measure the hot electron bremsstrahlung spectrum. The detector is sensitive to X-rays with energies ranging from 40 keV to the MeV range. The parallel-energy particle analyzer is a three-grid, electrostatic, electron flux collector constructed inside a 1" diameter copper tube placed in the opposite mirror end from the whistler wave launcher. Because of the small opening in the separation grids, 50 x 50 lines/inch^2 with 80% transparency, this analyzer is usually only sensitive to the parallel energy of the hot-electrons. Perpendicular energy can be measured by lowering the magnetic field strength near the analyzer so that a known fraction of the perpendicular energy is converted into parallel energy.

Other diagnostics, not shown in Fig. 7, include an axially moveable rf probe, a radially moveable Langmuir probe, an azimuthally movable ionization chamber probe and diamagnetic loops, etc. The rf probe signal is connected to a HP8551 spectrum analyzer for detailed spectral studies. The ionization chamber probe is sensitive to the flux of electrons with energies greater than 1.56 keV. The signal from this diagnostic is amplified by a sensitive electrometer and a synchronous detector, and is very useful in obtaining the heating rates of the hot particles. Most of the experimental data are interfaced to a PC/XT computer using board level ADC interface circuitry.

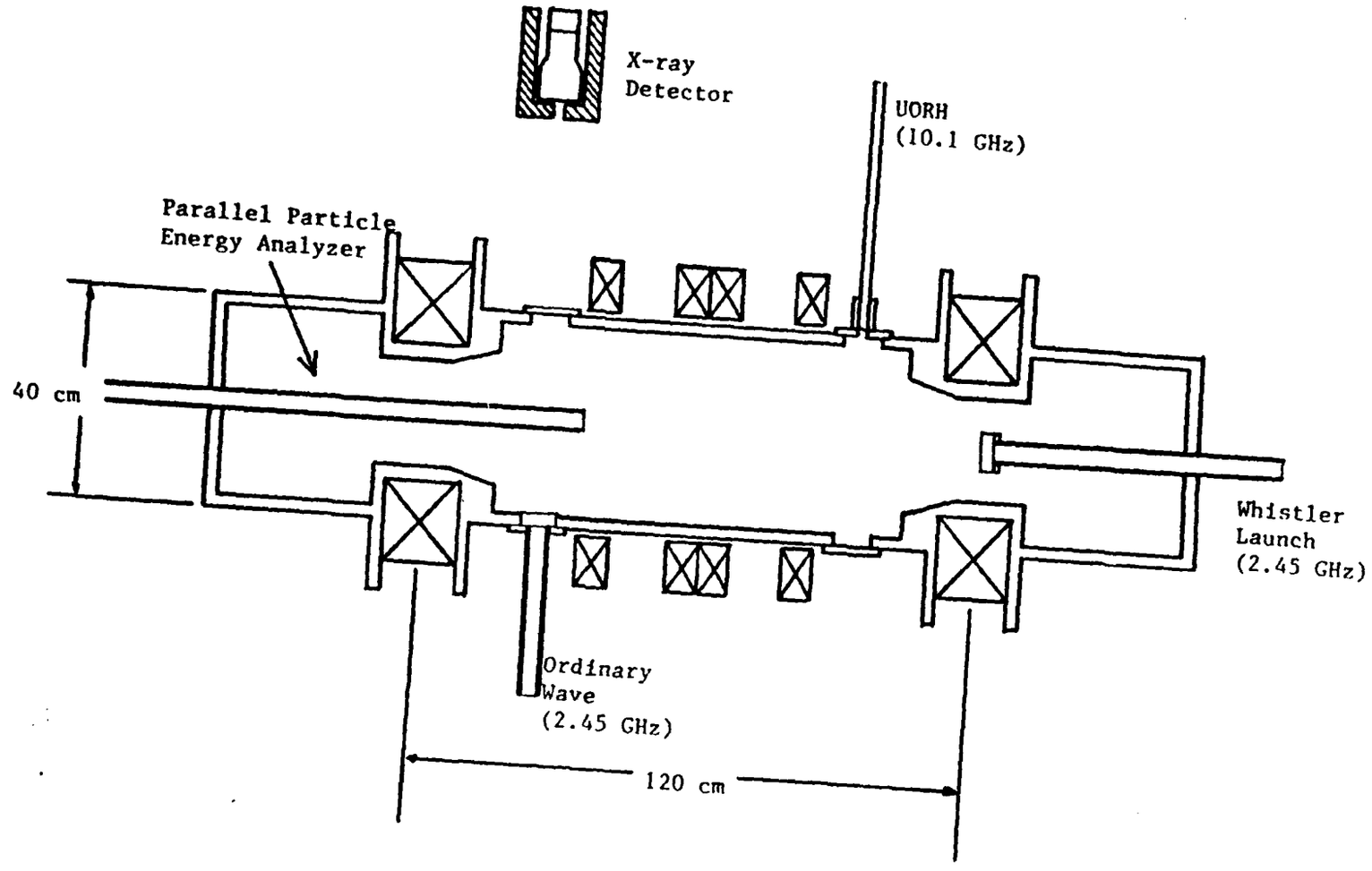

FIGURE 7: The schematic of the AMPHED facility and ECH experimental arrangement.

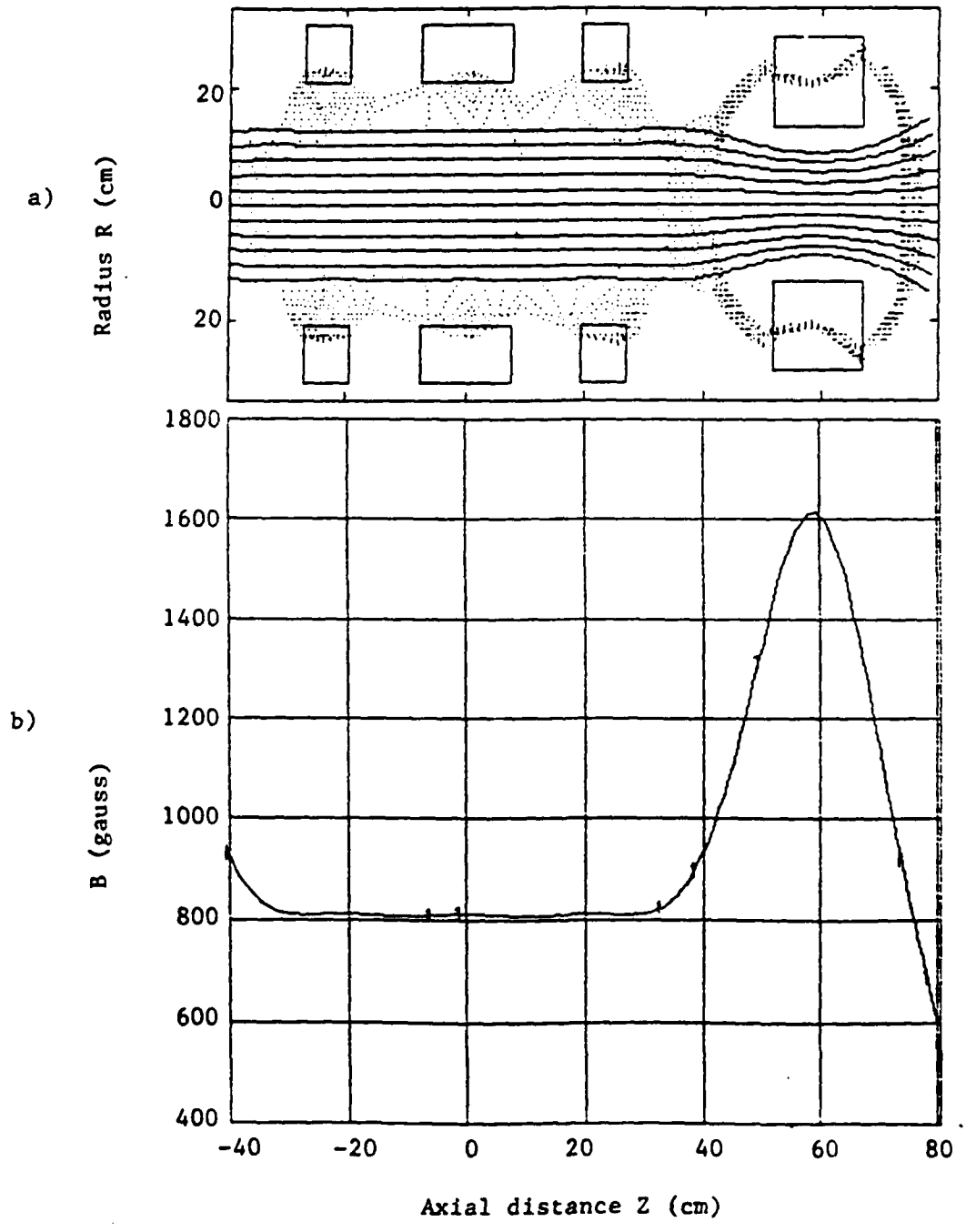

FIGURE 8: The magnetic field plot of AMPHED in the flat field configuration:

a) Magnetic field lines and mod-B contour plots for I_B = 200 Amps.

b) Field intensity vs axial position along the mirror axis.

3.2.3 Whistler wave injection

Microwave power launched from the high-field mirror throat is known to excite whistler waves with the propagation vector $\vec{k}$ parallel to the magnetic field lines. This was confirmed experimentally by measuring the spatial correlation function, $E_{\perp}(z)\cos[zk_{||}(z)]$, along the field direction using a moveable RF probe and a microwave interferometric technique, as shown in Figs. 9a and 9b. The local wavelength of the observed wave decreases rapidly as it propagates toward the resonance layer, in qualitative agreement with the whistler wave dispersion relation. (15)

$$n^2 = 1 - \alpha\omega/(\omega - \Omega \cos\theta)$$

where $n^2 = (kc/\omega)^2$ is the refractive index, $\alpha = (\omega_{pe}/\omega)^2$, $\Omega = eB/mc$, θ is the angle between the wave vector and the magnetic field lines, c is the speed of light, e is the electron charge, m is the electron mass, ω_{pe} is the electron plasma frequency, and ω is the angular frequency of the heating wave. We see that as Ω decreases and approaches ω at the ECR layer, n increases and approaches infinity, as observed in Fig. 9b. Notice that at $z \sim 5$ cm, $\Omega \sim 1.7\omega$. Using the measured value of $\alpha = 10$, we have from equation (1), $n^2 = 1 - 10\omega/(\omega - 1.7\omega) \sim 15$, or $\lambda_0/\lambda = 3.8$. This gives $\lambda = \lambda_0/3.8 = 3.2$ cm, in close agreement with the measured wavelength of 3.3 cm.

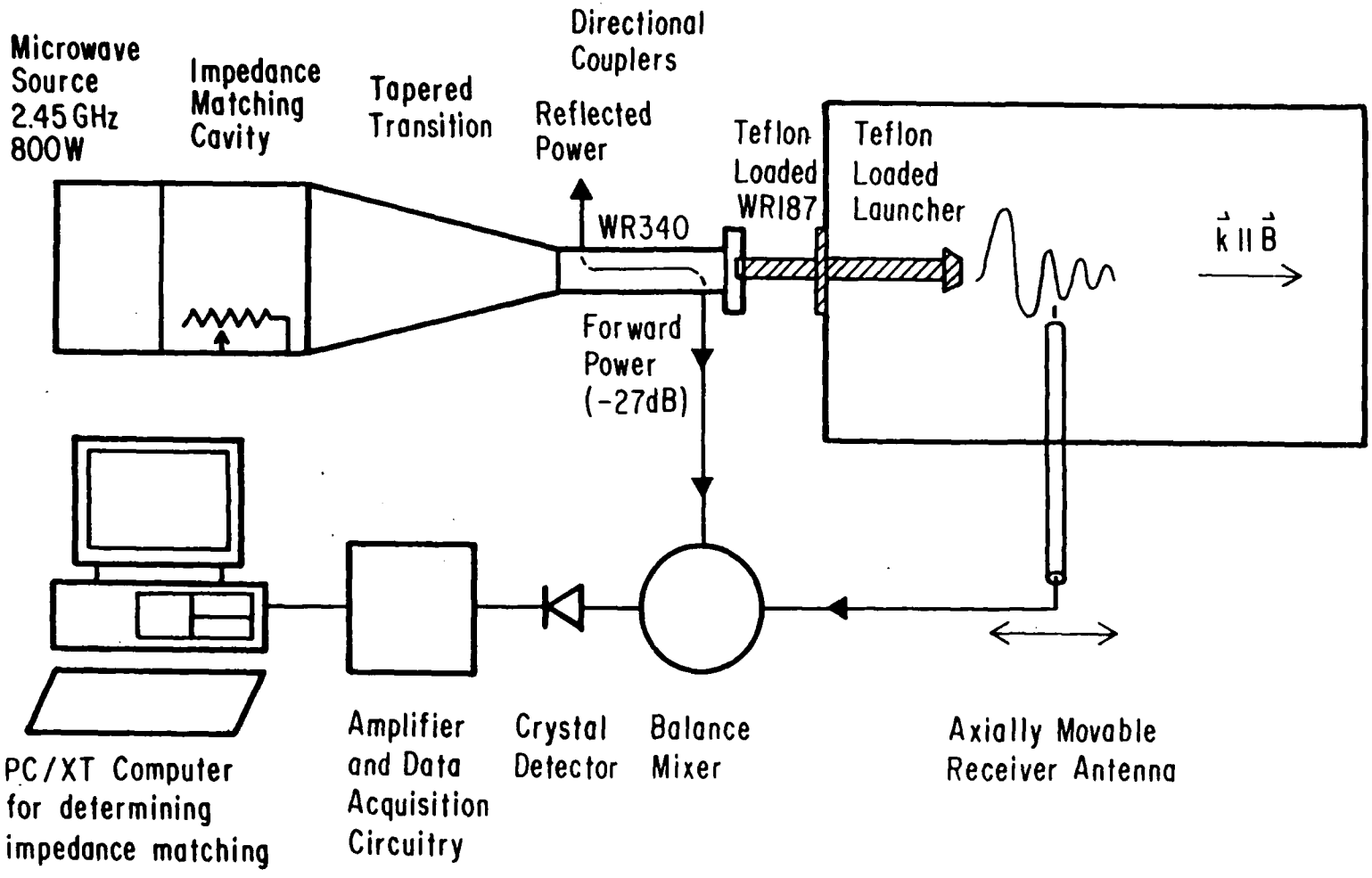

FIGURE 9a: Experimental arrangement used for launching and characterizing whistler waves in AMPHED.

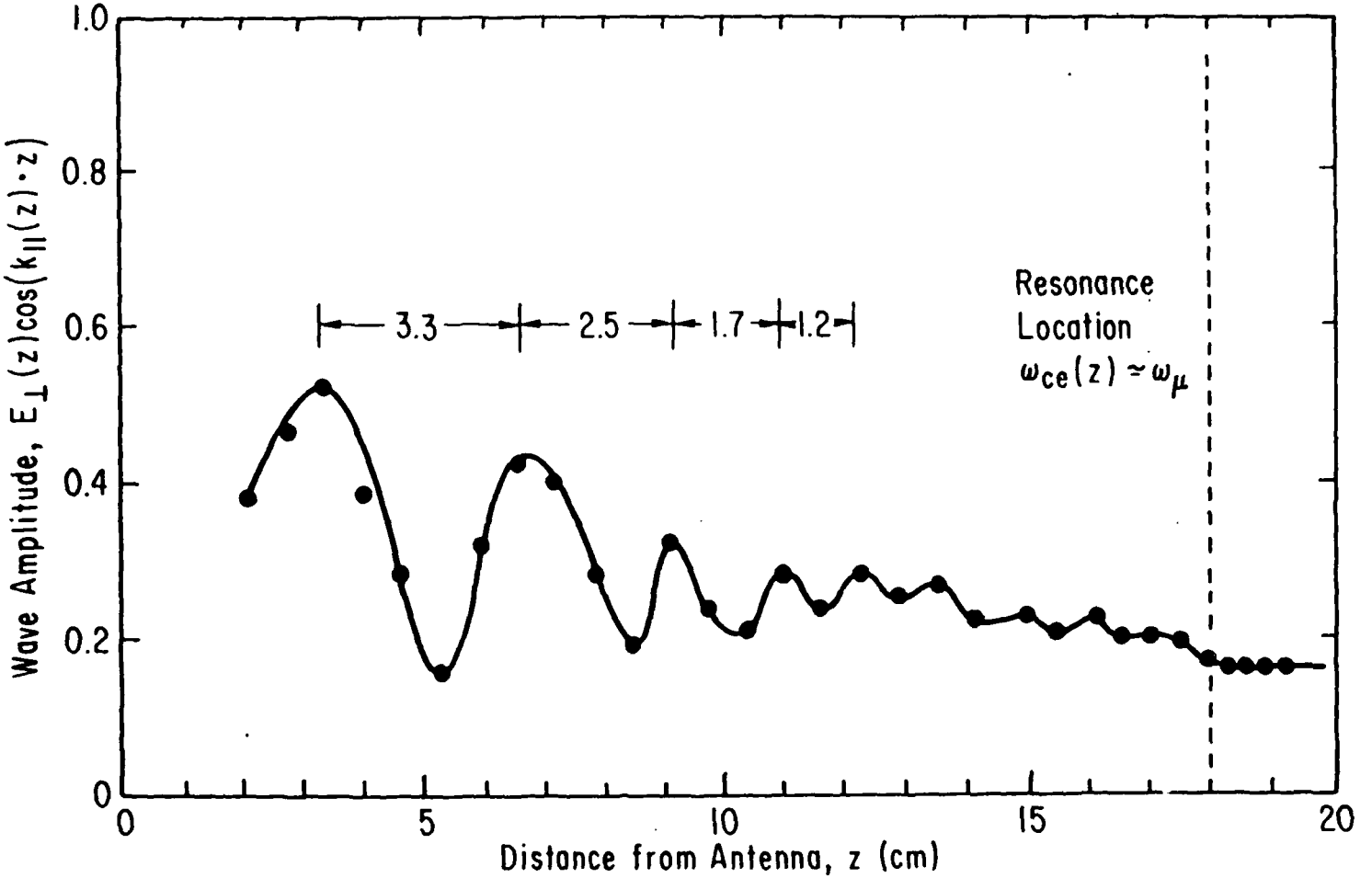

FIGURE 9b: Experimental measurement of the whistler-wave spatial waveform, showing decreasing wave length as the wave propagates toward the ECH layer.

SECTION 3.3

Amplification of whistler waves propagating through inhomogeneous, anisotropic, mirror-confined hot-electron plasmas

G. E. Guest and R. L. Miller
Applied Microwave Plasma Concepts, Inc., Carlsbad, California 92009

(Received 15 April 1988; accepted 18 August 1988)

A fully relativistic local dispersion relation for whistler waves has been solved at closely spaced points along the magnetic field lines of a 2:1 magnetic mirror in which a highly anisotropic, spatially inhomogeneous, hot-electron plasma is confined. The limiting plasma parameters for convective (spatial) growth have been determined numerically and used to identify plasma conditions leading to maximum amplification of input microwave signals introduced in the form of whistler waves. The maximum gain has been evaluated numerically for a range of values of the hot-electron plasma within which all major stability criteria are satisfied. Very high gains ($\sim$40 dB) are indicated over the entire range of beta investigated.

I. INTRODUCTION

It is well known that whistler waves can be unstable in mirror-confined hot-electron plasmas because of the pressure anisotropy inherent in magnetic-mirror confinement.[1] Indeed, the phenomenon of unstable whistler waves has often been invoked to interpret spontaneous rf emissions from laboratory[2] and space plasmas,[3] and has recently been proposed as a way of transforming the energy stored in mirror-confined hot-electron plasmas into giant pulses of high-powered microwave radiation.[4,5] The proposed transformation results from the amplification of whistler waves propagating along magnetic lines of force and passing through the anisotropic, hot-electron plasma. Here we investigate the maximum gain that a whistler can undergo in a spatially inhomogeneous plasma, confined in a magnetic-mirror field of finite spatial extent.

Because the whistler instability mechanism depends on the kinetic properties of the hot-electron equilibrium, particularly the distribution of electrons in velocity space, theoretical analyses of the growth typically use idealized, spatially uniform models of the plasma in order to treat the velocity-space issues realistically.[1] Under these idealized conditions, growth of the whistler wave can be either convective or absolute, depending on the plasma parameters.[6] Absolutely unstable or temporally growing waves are expected to spread throughout the unstable plasma and grow in amplitude until quasilinear or nonlinear processes balance the destabilizing conditions. By contrast, the growth of convectively unstable or spatially amplifying waves may be limited by the finite transit time of a wave packet across the finite spatial extent of the unstable plasma as well as by the spatial nonuniformity of the confining magnetic field, rather than quasilinear or nonlinear mechanisms.

In the present study we use linearized theories to determine the overall gain, $G(\omega)$, experienced by a pulse of microwave power launched at one end of a mirror-confined, hot-electron plasma and propagating along the magnetic lines of force in the form of whistler waves:

$$G(\omega) \equiv |E^2_{\text{out}}(\omega, z = +L)|/|E^2_{\text{in}}(\omega, z = -L)|.$$

Here ω is the (radian) frequency of the wave launched at the axial position $z = -L$ with rf electric field strength E_{in}. After a single transit through the plasma, the wave arrives at the axial position $z = L$ with amplitude E_{out}. Since this procedure will yield the desired gain only if the unstable growth is convective, we have carried out a detailed numerical evaluation of the threshold conditions for absolute growth and restricted the range of plasma parameters to lie entirely within the convectively unstable range.

Apart from transients at the beginning and end of each pulse, the input wave amplitude is assumed to be constant in time throughout the pulse; and the spatial and temporal behavior of the wave can be determined using Fourier and Laplace transformed equations in the conventional way.[6] When inverting the transformed variables it is necessary to displace the Laplace integral path to the real-ω axis while deforming the Fourier inversion path to prevent any zeros of the dispersion relation from crossing the deformed path of integration in the complex k plane, where k is the (parallel) wavenumber. As is well known, this procedure is only possible if the whistler wave growth is convective; in the case of absolute growth, two poles from opposite halves of the complex k plane merge.

To ensure that we consider only convectively unstable cases, we have evaluated the threshold conditions for absolute (temporal) growth for the hot-electron equilibria under investigation. For hot-electron plasmas created by electron cyclotron heating (ECH), the convective/absolute boundary can be conveniently represented in two dimensions by fixing some of the plasma parameters in ways that reflect fundamental properties of the ECH process. Thus, for example, the total plasma density is usually limited by microwave cutoff so that $\omega^2_{p_e}/\omega^2_{\mu} \leq 1$. Here ω_{p_e} and ω_{μ} are the electron plasma and microwave frequencies, respectively. Moreover, the relative density of hot electrons $n_h/n \equiv \Delta$ may be limited by the onset of flutelike instabilities in simple magnetic-mirror configurations; although no such limitation occurs in magnetic "well" configurations with favorable curvature of the magnetic lines of force. Even in such a flute-stable configuration, however, the plasma pressure may be limited by equilibrium conditions such as the so-called "mirror mode," and the value of hot-electron beta, $\beta = 2\mu_0 P_h/B^2$, may be limited in inverse proportion to the anisotropy.[7] Here B is the magnetic intensity and μ_0 is the permeability of free space.

 0031-9171/88/123690-07$01.90

If no other stability criteria are violated, the gain $G(\omega)$ can be evaluated up to the threshold conditions defined by the C/A boundary in a straightforward way; this is the main objective of the work described here. The gain is then given directly by

$$G(\omega) = \exp\left(-2 \int_{-L}^{L} k_i(\omega,z)dz \right),$$

where k_i is the imaginary part of the wave vector corresponding to solutions of the local dispersion relation with real frequency ω.

In order to account for the z-dependent equilibria confined in finite sized magnetic-mirror configurations we adopt simple model equilibria with hot-electron distribution functions mapped along magnetic field lines through adiabatic invariants. The properties of these equilibria are summarized briefly in Sec. II. A fully relativistic dispersion relation is then used to evaluate the C/A boundary for whistler waves. The dispersion relation, while fully relativistic, can give only a local evaluation of the wave properties, since it is derived under the assumptions of spatial uniformity. This procedure is expected to yield a valid description provided the scale length for variation of the plasma equilibrium is much greater than the wavelength of the whistler waves. Since we are primarily interested in quasioptical systems with scale lengths much larger than wavelengths, this condition is not particularly restrictive. In effect, we are constructing a WKB solution from numerical solutions of the local dispersion relation within plasma parameter ranges for which the unstable growth is guaranteed to be convective. The numerical analysis of the dispersion relation and typical results are recapitulated in Sec. III. The gain is then evaluated from real-ω solutions of the dispersion relation in a way that is discussed at some length in Sec. IV. Several cases are presented there in which the temperature anisotropy and hot-electron beta are varied so as to move along a particular C/A boundary (corresponding to a fixed relative hot-electron concentration, $\Delta = 30\%$). Substantial values of the gain are indicated for hot-electron plasmas of typical laboratory dimensions.

The major findings are summarized in Sec. V, and the nature of these findings is discussed. In particular, the unresolved issue of the role of quasilinear or nonlinear processes is given some emphasis because of the indications that the maximum gain predicted in the linear theory varies only weakly with beta and remains large in plasmas with high energy densities, where saturation levels of output power might be expected to be very high.

II. THE MODEL EQUILIBRIA

In this section we summarize the way in which the equilibrium properties of the plasma depend on distance along the magnetic lines of force. Local properties of electron cyclotron heated hot-electron plasmas have been discussed extensively,[7] and a few studies have attempted to model the axial dependence in nonrelativistic formulations of the hot-electron dynamics. Here we follow the conventional approach to mapping relativistic-electron equilibria along magnetic lines of force assuming the invariance of the total energy ϵ, and the magnetic moment μ:

$$\epsilon = mc^2(\gamma - 1) = mc^2\left[\sqrt{1 + (u^2/c^2)} - 1\right]$$

and

$$\mu = (m\mu_\perp^2)/(2B).$$

In these expression, γ is the relativistic Lorentz factor and $\mathbf{u}$ is the momentum per unit rest mass with components $u_\perp$ and $u_\parallel$ perpendicular and parallel, respectively, to the magnetic field $\mathbf{B}$. Here m is the electron rest mass and c is the speed of light in vacuum.

The relative intensity of the steady magnetic field is assumed to vary along the line of force of interest as follows:

$$b = \frac{B(z)}{B(0)} = \left(\frac{M+1}{2}\right) - \left(\frac{M-1}{2}\right)\cos\left(\frac{\pi z}{L}\right).$$

Here $z = 0$ defines the so-called "midplane" on which the magnetic intensity reaches its minimum value $b = 1$, while $z = L$ defines the so-called "mirror throat," where B reaches its maximum value $b = M$, the mirror ratio.

The cold-electron component, which typically contains the majority of electrons, will be modeled as an isotropic, pressureless fluid whose density is independent of z. By contrast, the hot-electron component is assumed to be anisotropic and relativistic and described by a distribution function of the form[8]

$$f_h(u_\perp^2,u_\parallel^2,z) = \begin{cases} \sum_{l=0}^{\infty} C_h^{(l)} \left(\frac{u_\perp^2}{b\alpha_\perp^2}\right)^l \exp\left\{ -\left(\frac{u_\parallel^2}{\alpha_\parallel^2} + (b-1)\frac{u_\perp^2}{b\alpha_\parallel^2} + \frac{u_\perp^2}{b\alpha_\perp^2}\right)\right\}, & \text{outside of the loss cone,} \\ 0, & \text{inside the loss cone.} \end{cases} \quad (1)$$

If $\mathbf{u}_0$ is the momentum per unit rest mass evaluated at the midplane $z = 0$, then in terms of the constants of motion,

$$u_{0\parallel}^2 = u^2 - 2\mu B_0/m = u_\parallel^2(z) + (b-1)[u_\perp^2(z)]/b \quad (2)$$

and

$$u_{0\perp}^2 = 2\mu B_0/m = u_\perp^2/b. \quad (3)$$

Here $u_{0\parallel}$ and $u_{0\perp}$ are the components of $\mathbf{u}_0$ parallel and perpendicular, respectively, to the static magnetic field.

A z-dependent loss cone in $\mathbf{u}$ space is defined by setting

$u_\parallel^2(L) = 0$:

$$u_\parallel^2(L) = u^2 - 2\mu B_{max}/m = 0$$
$$= u_\parallel^2(z) + u_\perp^2(z) - u_\perp^2(z)B_{max}/B(z),$$

or

$$\left(\frac{u_\parallel^2(z)}{u_\perp^2(z)}\right)_{\text{loss cone}} = \frac{B_{max}}{B(z)} - 1 = \frac{M}{b} - 1. \quad (4)$$

If we now collect terms in $u_\perp^2(z)$ in the exponential factor we have

$$f_h(u_\perp^2, u_\parallel^2, z) = \sum_{l=0}^{\infty} C_h^{(l)} \left(\frac{u_\perp^2}{b\alpha_\perp^2}\right)^l \exp\left(-\frac{u_\parallel^2}{\alpha_\parallel^2} - \frac{u_\perp^2}{\alpha_\perp^2(z)}\right),$$
$$\text{if } \frac{u_\parallel^2}{u_\perp^2} < \frac{M}{b-1}, \quad (5)$$
$$= 0, \quad \text{if } \frac{u_\parallel^2}{u_\perp^2} > \frac{M}{b-1},$$

where

$$\alpha_\perp^2(z) = (\alpha_{\perp 0}^2 \alpha_\parallel^2 b)/[\alpha_{\perp 0}^2(b-1) + \alpha_\parallel^2],$$

or, if $\eta \equiv \alpha_{\perp 0}^2/\alpha_\parallel^2$,

$$\alpha_\perp^2(z) = \eta b \alpha_\parallel^2/[\eta(b-1)+1]. \quad (6)$$

The z-dependent hot-electron density is now given by

$$n_h(z) = \sum_{l=0}^{\infty} C_h^{(l)} \pi \int_{-\infty}^{\infty} du_\parallel \exp\left(-\frac{u_\parallel^2}{\alpha_\parallel^2}\right)$$
$$\times \int_{bu_\parallel^2/(M-b)}^{\infty} du_\perp^2 \left(\frac{u_\perp^2}{b\alpha_\perp^2}\right)^l \exp\left(-\frac{u_\perp^2}{\alpha_\perp^2(z)}\right), \quad (7)$$

and for the simple bi-Gaussian distribution, $l = 0$, we have

$$n_h(z) = \pi^{3/2}\alpha_\perp^2(z)\alpha_\parallel C_h^{(0)}\{1 + [\alpha_\parallel^2/\alpha_\perp^2(z)]$$
$$\times [b/(M-b)]\}^{-1/2} \quad (8)$$

or

$$\frac{n_h(z)}{n_h(0)} = \frac{\alpha_\perp^2(z)}{\alpha_{\perp 0}^2}\left(1 + \frac{(\alpha_\parallel^2/\alpha_{\perp 0}^2)\,[1/(M-1)]}{1 + [\alpha_\parallel^2/\alpha_\perp^2(z)]\,[b/(M-b)]}\right)^{1/2}$$
$$= \frac{b}{\eta(b-1)+1}\sqrt{\frac{(M-b)}{(M-1)}}. \quad (9)$$

An illustrative case is shown in Fig. 1 for a mirror ratio $M = 2$ and two different temperature anisotropies, $\eta = 5$ and 20. The z-dependent relative magnetic intensity b is shown, together with the z-dependent relative hot-electron densities for the two different temperature anisotropies. The figure indicates the degree to which higher temperature anisotropy is associated with increased peaking of the hot-electron density at the midplane. This property of the equilibria will be shown to have a major impact on the overall gain of a whistler wave propagating along the magnetic line of force. In quantitative terms, the z dependence of hot-electron density is given by

$$\frac{d}{dz}\frac{n_h(z)}{n_h(0)} = \frac{db}{dz}\left(\frac{(1-\eta)}{[1+\eta(b-1)]^2}\sqrt{\frac{(M-b)}{(M-1)}}\right.$$
$$\left. - \frac{b}{2\sqrt{(M-1)(M-b)}}\frac{1}{1+\eta(b-1)}\right)$$
$$\to \frac{db}{dz}\left(1 - \eta - \frac{1}{2(M-1)}\right), \quad \text{as } b \to 1. \quad (10)$$

Although it is not included in Fig. 1, the temperature anisotropy also decreases with distance from the midplane as

$$\frac{\alpha_\perp^2(z)}{\alpha_\parallel^2} = \frac{\eta b}{1+\eta(b-1)},$$

so that

$$\frac{d\alpha_\perp^2}{dz} = \frac{\alpha_\parallel^2 \eta b'(1-\eta)}{[1+\eta(b-1)]^2}. \quad (11)$$

Thus both temperature anisotropy and the relative hot-electron density decrease with distance away from the midplane, so that maximum amplification will occur at the midplane.

In contrast to this strong z dependence of the hot-electron density, the cold-electron density is expected to remain nearly constant in z, except for the spatial compression associated with the increasing magnetic intensity. The real value of $k(\omega)$ is determined mainly by the cold-plasma density and the magnetic intensity, and is slowly varying along the magnetic field lines.

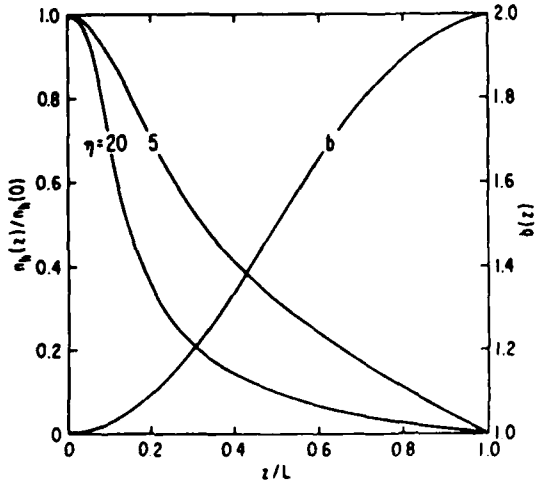

FIG. 1. Variation of relative hot-electron density and magnetic intensity, b, with distance along a magnetic field line.

III. CONDITIONS FOR MAXIMUM GAIN

The maximum amplification of an externally launched whistler wave is likely to be achieved in hot-electron plasmas that are just below the threshold for absolute or temporal growth. This threshold is frequently referred to as the C/A boundary, which is a hypersurface in a space spanned by the plasma parameters. On one side of this boundary only convective or spatial growth is possible, while on the opposite side of the boundary, absolute or temporal growth occurs. Thus, in order to explore the maximum gain that can be achieved, it is first necessary to define the C/A boundary in

terms of equilibrium parameters representative of physically realizable plasmas. This section summarizes the results of a numerical determination of the C/A boundary for unstable whistler waves in hot-electron plasmas whose local properties are modeled by the class of infinite, homogeneous, relativistic-electron distribution functions cited earlier, namely,

$$f_n = \sum_{l=0}^{\infty} C_l \left(\frac{u_\perp}{\alpha_\perp}\right)^{2l} e^{-u_\perp^2/\alpha_\perp^2} e^{-u_\parallel^2/\alpha_\parallel^2}.$$

The general methodology adopted here for determining the C/A boundary has been discussed at length by Briggs[6] and consists ultimately in locating simultaneous solutions of the dispersion relation and its derivative with respect to k, the (complex) wavenumber, for real values of the frequency ω. This general methodology is implemented in our case through novel numerical techniques appropriate to the class of distribution functions used here. These techniques have been fully described by Guest and Miller.[9]

It has been well established by many investigators[1] that the growth rate of unstable whistler waves increases with increasing values of the temperature anisotropy and the hot-electron beta, where beta is the ratio of the kinetic pressure nT to the magnetostatic pressure $B^2/2\mu_0$. For hot-electron plasmas created by electron cyclotron heating (ECH), several fundamental aspects of the heating and confinement processes limit the physically accessible values of beta and anisotropy in ways that can usefully restrict the range of plasma parameters to be considered here.[7,9] For example, effective penetration of the ECH power typically limits the maximum (total) electron density to values such that $\omega_{pe}^2 < \omega_\mu^2$, where ω_μ is the angular frequency of the ECH power. Typically, the relative fraction of electrons heated to high energies, $\Delta = n_h/n$, is much less than unity. Idealized theories of flutelike instabilities have been used to estimate critical values of Δ set by thresholds for occurrence of flutelike or ballooning modes: $\Delta_{crit} \sim 0.3$. Relativistic effects appear to increase this substantially, but we will usually assume $\Delta \leq 0.5$. In small magnetic mirrors, nonadiabatic effects can limit the maximum hot-electron energy to values such that $\rho \leq 0.05L$. Here ρ is the (relativistic) electron gyroradius and L is a characteristic scale length of the magnetic geometry. The condition for equilibrium, sometimes referred to as the mirror instability criterion, limits the product of anisotropy and beta, roughly as $\beta(\eta - 1) < 1$. For the anisotropic, hot-electron distribution functions used in the present work, a more accurate estimate of the beta limit corresponding to the mirror criterion can be obtained from the more general condition for existence of equilibria[10]:

$$\tau \equiv \frac{1}{\mu_0} + \frac{1}{B}\frac{dp_\perp}{dB} > 0. \tag{12}$$

In the nonrelativistic approximation, $p_\perp$, the component of plasma pressure perpendicular to the static magnetic field, is given by

$$p_\perp = mn\langle v_x^2\rangle = mn\langle v_y^2\rangle = mn\langle v_\perp^2/2\rangle$$
$$= \pi \int_{-\infty}^{\infty} dv_\parallel \int_{v_{\perp lo}}^{\infty} v_\perp \, dv_\perp \, f(v_\perp, v_\parallel) m v_\perp^2. \tag{13}$$

Here $v_{\perp lo}^2 = v_\parallel^2 b/(M-b)$ defines the loss cone at the point z where the local magnetic intensity is $B = bB_0$. Note that $v_{\perp lo}^2 \to 0$ as $M \to \infty$. If we use the bi-Maxwellian distribution function corresponding to $l = 0$[8] and evaluate the derivative of $p_\perp$ at the midplane, we obtain from the mirror criterion

$$\beta_{\perp 0} \leq \frac{\sqrt{M-1}(\eta^{-1} + M - 1)^{3/2}}{(M-1)(\eta - 1)(1.5\eta^{-1} + M - 1) - 3\eta^{-1}/8}. \tag{14}$$

where $\eta \equiv \alpha_\perp^2/\alpha_\parallel^2$. We have evaluated the limiting value of $\beta_\perp(\eta)$ for $M = 2$ and displayed this boundary in Fig. 2. Note that as $M \to \infty$ this criterion approaches

$$\beta_\perp(\eta - 1) < 1.$$

In Fig. 2 we show the value of anisotropy on the convective/absolute boundary $\eta_{C/A}$ as a function of $\beta_\perp$ for conditions that are appropriate to an ECH-generated hot-electron plasma. We have set $\omega_{pe}^2/\omega_{ce}^2 = 1$ and $\Delta = 0.3$, and varied $\bar{\gamma}$ to cover the indicated range of values of $\beta_\perp$. The associated values of $\bar{\gamma}$ are shown by the curve labeled $\bar{\gamma} - 1$. Here $\bar{\gamma}$ is the average of γ over the equilibrium distribution function, Eq. (5), in which only the $l = 0$ component is retained. The approximate mirror instability criteria $\beta(\eta - 1) = 1$ and $\tau = 0$ are also shown here; note that the C/A boundary lies slightly above the equilibrium limit for $\beta_\perp \geq 10\%$–20%. The nonrelativistic C/A boundary given by Iiyoshi *et al.*[11] is also shown for comparison with the fully relativistic numerical results. For a given value of $\beta_\perp$ the relativistic expressions indicate that slightly higher values of anisotropy are required for absolute growth.

The C/A boundary shown in Fig. 2 satisfies the conditions for physical accessibility identified here for $\beta_\perp \leq 10\%$–20% and thus will be used to estimate the maximum gain that can be achieved at lower values of beta. The results of

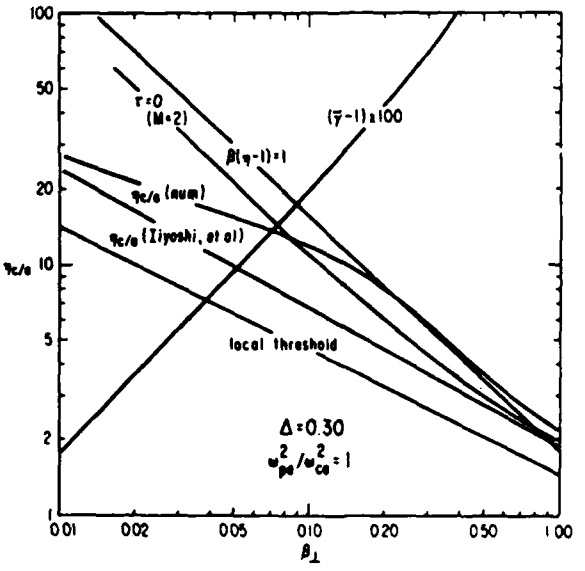

FIG. 2. Variation of anisotropy of the C/A boundary, $\eta_{c/a}$, and average hot-electron energy, $\bar{\gamma}$, with $\beta_\perp$, the perpendicular hot-electron beta. Here $\omega_{pe}^2/\omega_{ce}^2 = 1$ and $\Delta = 0.3$. Also shown is the mirror instability threshold.

this evaluation of gain are described in Sec. IV.

We conclude the present section with one further set of results on the local wave properties of unstable whistlers at the C/A boundary shown in Fig. 2. These are displayed as functions of $\beta_\perp$ in Fig. 3, where we see that both the real and imaginary components of the propagation vector, together with the wave frequency, are decreasing functions of beta. This decrease reflects two underlying facets of the C/A boundary along which the parameters are evaluated, namely, that the maximum anisotropy for convective growth is decreasing with increasing values of beta, and that, in the present case, beta is being increased by increasing the average electron energy and hence the relativistic mass shift. The relativistic effects can be removed by holding the hot-electron energy fixed and varying beta by varying Δ. This procedure has been followed in generating the results shown in Figs. 4 and 5.

Figure 4 again shows the anisotropy at the C/A boundary as a function of beta, together with the corresponding values of Δ and the mirror instability criterion for $\bar{\gamma} = 1.4$. This value of $\bar{\gamma}$ corresponds to an average hot-electron energy just above 100 keV ($T = 111$ keV). Note that absolute growth is only possible for $\beta_\perp > 0.10$ corresponding to $\Delta = 0.155$, and that the C/A boundary drops below the mirror stability limit for $\beta_\perp > 0.17$ or $\Delta > 0.27$. The wave parameters along the C/A boundary are shown in Fig. 5, and here reflect only the decreasing value of anisotropy, as well as the increasing value of Δ. In the range that satisfies the mirror stability criterion, the wave parameters decrease only slightly, suggesting that relativistic effects are mainly responsible for the large decrease in wave parameters shown in Fig. 3.

IV. EVALUATION OF MAXIMUM GAIN

We now estimate the maximum achievable gain for various plasma parameters by numerically evaluating the integral along magnetic field lines of the imaginary part of the propagation vector:

$$\ln G(\omega) = -2\int_{l_-}^{l_+} k_i(\omega,z)\,dz. \tag{15}$$

This procedure is valid provided the growth is convective. We will examine a sequence of cases in which the plasma beta is increasing, and for each value of beta we will assume the maximum anisotropy for which the whistler growth is convective. Since the plasma density and anisotropy are greatest on the midplane, it is the midplane values of plasma

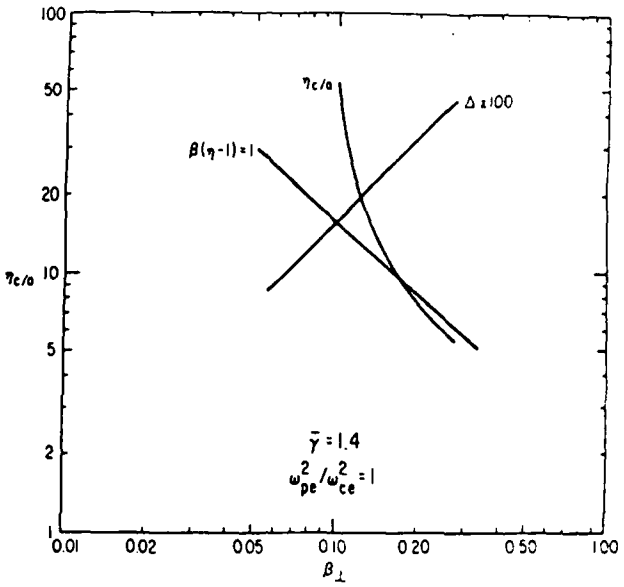

FIG. 4. The C/A boundary for fixed $\bar{\gamma} = 1.4$ and the relative hot-electron density, Δ, together with the mirror instability criterion.

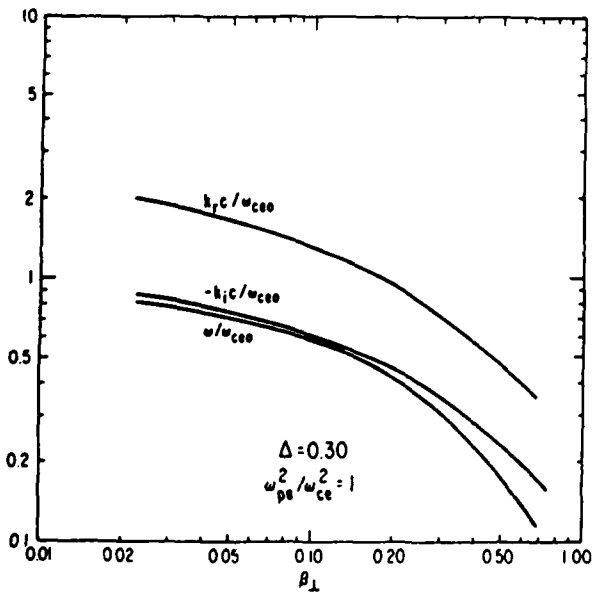

FIG. 3. Wave parameters versus $\beta_\perp$ for $\eta_{c/A}$ on the C/A boundary shown in Fig. 2.

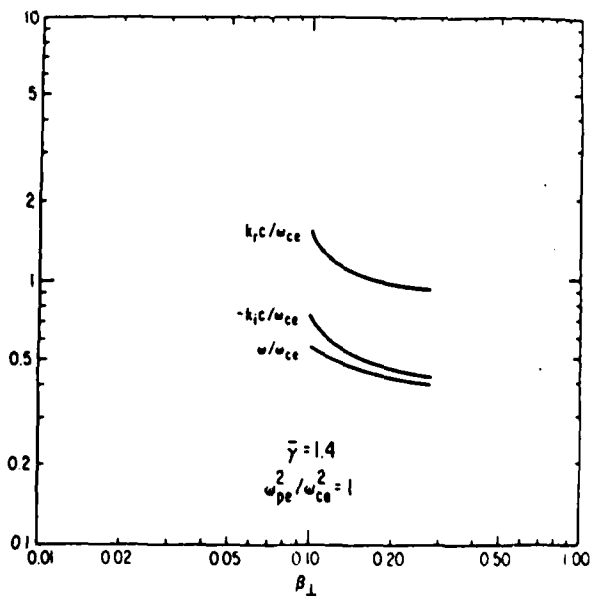

FIG. 5. Wave parameters along the C/A boundary for the cases shown in Fig. 4.

and wave parameters on the C/A boundary that determine the maximum anisotropy and the corresponding wave frequency for each value of beta. The anisotropy and density are readily determined at each point along the magnetic field line; and the dispersion relation is then solved locally to obtain the complex propagation vector at that point for the frequency specified at the midplane. The gain integral is then evaluated numerically.

We have carried out this evaluation of the gain for $\beta_\perp \doteq 5\%$, 10%, 15%, 20%, and 25% in the case shown in Fig. 2: $\omega_{pe}^2/\omega_{ce}^2 = 1$, $\Delta = 0.30$, and $l = 0$. The magnetic geometry assumed was a fixed $M = 2$ magnetic mirror; and thus no attempt was made to relate the equilibrium value of the anisotropy to the shape of the magnetic field. We return to this point in Sec. V. The midplane parameters for the cases examined are tabulated in Table I. The series was terminated at $\beta_\perp = 25\%$ since the mirror instability criterion was not satisfied at the C/A boundary for greater values of $\beta_\perp$.

The last column of Table I gives the value of

$$I \equiv -\int_0^1 \left(\frac{k_i c}{\omega_{ce0}}\right)\left(\frac{dz}{L}\right).$$

The gain is then given by

$$G(\omega) = \exp[4(L\omega_{ce0}/C)I].$$

For typical conditions, the applied microwave power resonates with the second harmonic of the local electron gyrofrequency at the midplane. Thus

$$\omega_{ce0} = \pi f_\mu,$$

and we can estimate the scale factor as follows:

$$\frac{4L\omega_{ce0}}{c} \simeq \frac{4\pi L f_\mu}{c} = \frac{4\pi L}{\lambda_\mu},$$

where λ_μ is the free-space wavelength of the microwave heating power. In order of magnitude, $L/\lambda_\mu \gtrsim O(10)$ for typical existing experimental devices. The indicated values of gain are then, again, in order of magnitude,

$$G(\omega) \sim O(10^4) \sim 40 \text{ dB}.$$

In addition to the peak growth rates shown in Table I we can readily estimate the effective bandwidth by calculating the total gain for whistler waves of varying frequencies propagating through a particular anisotropic, mirror-confined, hot-electron equilibrium. For definitiveness, we again choose the plasma parameters to be near the convective/absolute boundary for the center frequency of the unstable frequency band. Illustrative cases of $\beta_\perp = 5\%$, 10%, and 20% are shown in Fig. 6, where the dimensionless gain factor,

$$-\int_0^L \left(\frac{k_i c}{\omega_{ce0}}\right)\frac{dz}{L},$$

is plotted against the frequency normalized to the center frequency. Note that the bandwidth increases as $\beta_\perp$ increases, i.e., as the average hot-electron energy increases. The full-width at half-maximum varies from roughly 0.15 at $\beta_\perp = 5\%$ to more than 0.25 at $\beta_\perp = 20\%$.

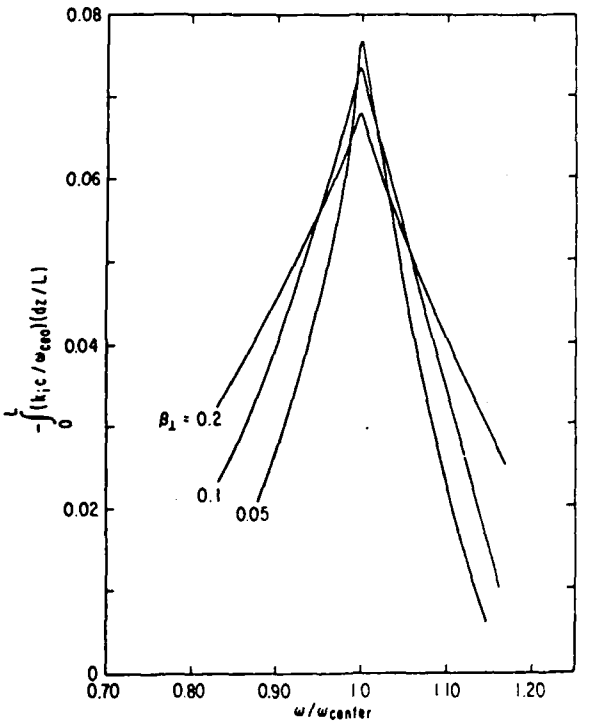

FIG. 6. The frequency-dependent gain factor, $-\int_0^L (k_i c/\omega_{ce0})dz/L$, for whistler waves of varying frequency in hot-electron equilibria with temperature anisotropies near the convective/absolute boundary and $\beta_\perp \doteq 5\%$, 10%, and 20%. Plasma and wave parameters for these three cases are listed in Table I.

Thus the linear theory suggests that very high gain is possible. It should be emphasized that the linear theory can-

TABLE I. Summary of the wave and plasma parameters at the C/A boundary for varying values of $\beta_\perp$. For all these cases, $\omega_{pe}^2/\omega_{ce0}^2 = 1$ and $\Delta = 0.30$.

$\beta_\perp$ (%)	$\eta_{C/A}$	ω/ω_{ce0}	$k_r c/\omega_{ce0}$	$-k_i c/\omega_{ce0}$	$\bar{\gamma}$	$-\int_0^1 \frac{k_i c}{\omega_{ce0}}\frac{dz}{L}$
5	15.26	0.6998	1.623	0.7267	1.093	0.076
10	11.83	0.5769	1.316	0.5964	1.197	0.073
15	9.63	0.4840	1.093	0.5150	1.3125	0.070
20	7.972	0.4095	0.9357	0.4487	1.4375	0.067
25	6.698	0.3484	0.8109	0.3942	1.572	0.064
30	5.724	0.2977	0.7097	0.3485	1.717	...
35	4.988	0.2562	0.6280	0.3106	1.870	...
40	4.426	0.2220	0.5617	0.2787	2.031	...

not provide any indication of the maximum output power or, equivalently, the saturation value of the input power. These must be obtained from quasilinear or nonlinear models of the energy transformation process.

It is, in fact, most striking that the gain decreases only very slowly with increasing beta; one would expect that the maximum output power would be proportional to beta. As we remarked earlier, the fact that the spatial growth rate decreases with beta is in part attributable to the somewhat arbitrary assumption of fixed Δ. Beta is then proportional to the average energy of the hot electrons, and relativistic effects reduce the growth rates. Perhaps more important to the weak beta dependence of the gain is the fact that at low beta the C/A boundary permits very high anisotropy. High anisotropy, in turn, leads to very large spatial growth rates near the midplane. Although lower anisotropy does lead to less peaking of the density near the midplane, the growth is greatly reduced away from the midplane by the increased local magnetic field strength: ω/ω_{ce} is too small to permit large local growth rates.

V. CONCLUSIONS

In Sec. IV we demonstrated that the amplification of an externally launched whistler wave can exceed 40 dB over a relatively wide range of values of beta, $5\% \leqslant \beta_{\parallel} \leqslant 25\%$, for typical ECH plasma parameters: $\omega_{pe}^2/\omega_{ce}^2 = 1$, $\Delta = n_h/n = 0.3$, and $1.1 \leqslant \tilde{\gamma} \leqslant 1.6$. The corresponding limiting values of temperature anisotropy were $15 \geqslant \eta_{C/A} \geqslant 6$. These values of anisotropy are much larger than expected in a typical ECH plasma confined in a 2:1 magnetic mirror. Dandl[4] has proposed the use of adiabatic compression to increase η to the C/A boundary value. We have not attempted to include adiabatic compression in the present studies. The gain calculation included the strong spatial variation in hot-electron density and anisotropy, together with the spatial variation in the underlying 2:1 magnetic-mirror field. We conclude from these findings that strong amplification is possible for representative hot-electron equilibria in the linear regime; i.e., for input signals below some power level at which quasilinear or nonlinear effects will saturate the growth of the whistler wave. Clearly the linear theory cannot provide an estimate of this critical parameter; some type of quasilinear calculation of the saturation of whistler growth is required to address this issue.

Existing quasilinear studies of unstable whistler waves in infinite homogeneous plasmas have indicated that, within that highly idealized model, roughly 10% of the hot-electron energy can be transformed into wave energy before the growth rate is reduced to zero. If these estimates provide a valid indication for finite, inhomogeneous, mirror-confined plasmas, it would appear entirely feasible, by operating at higher values of beta in high field strength magnetic fields to achieve very high output power levels. In fact, it may well be that the infinite homogeneous quasilinear model provides an underestimate of the saturation power, since resonant electrons can escape a real magnetic mirror after giving a substantial fraction of their perpendicular kinetic energy to the wave. In effect, a nearly constant level of anisotropy is automatically maintained in an actual magnetic mirror, whereas the infinite, homogeneous quasilinear model allows the anisotropy to decrease as a result of the wave growth.

ACKNOWLEDGMENT

This research was supported by the U.S. Air Force Office of Scientific Research under Contract No. F49620-86-C-0055.

[1] R. N. Sudan, Phys. Fluids 6, 57 (1963); R. Z. Sagdeev and V. D. Shafranov, Sov. Phys. JETP 12, 130 (1961); N. T. Gladd, Phys. Fluids 26, 974 (1983), and references cited therein.

[2] See, for example, H. Ikegami, H. Ikezi, M. Hosokawa, K. Takayama, and S. Tanaka, Phys. Fluids 11, 1061 (1968); H. J. Booske, W. D. Getty, R. M. Gilgenbach, and R. H. Jong, *ibid.* 28, 3166 (1985); and references cited in these two works.

[3] C. F. Kennel and H. E. Petschek, J. Geophys. Res. 71, 1 (1966); see P. A. Bespalov and V. Yu. Trakhtengerts, in *Reviews of Plasma Physics*, edited by M. A. Leontovich (Consultants Bureau, New York, 1986), Vol. 10, p. 155, for an excellent review and substantial bibliography of the Soviet literature.

[4] R. R. Dandl, U.S. Patent No. 4 733 122 (22 March 1988).

[5] A. V. Gaponov-Grekhov, V. M. Glagolev, and V. Yu. Trakhtengerts, Sov. Phys. JETP 53, 1146 (1982).

[6] See, for example, R. J. Briggs, *Electron Stream Interaction With Plasmas* (MIT Press, Cambridge, MA, 1963).

[7] See, for example, G. E. Guest and D. J. Sigmar, Nucl. Fusion 11, 151 (1971).

[8] G. E. Guest and R. R. Dory, Phys. Fluids 8, 1853 (1965).

[9] G. E. Guest and R. L. Miller, Nucl. Fusion 28, 419 (1988).

[10] H. Grad, Phys. Fluids 9, 225 (1966).

[11] A. H. Iiyoshi, H. Yamato, and S. Yoshikawa, Phys. Fluids 10, 749 (1967).

SECTION 3.4

FORMATION OF STABLE, HIGH-BETA, RELATIVISTIC-ELECTRON PLASMAS USING ELECTRON CYCLOTRON HEATING

G.E. GUEST, R.L. MILLER
Applied Microwave Plasma Concepts, Inc.,
Carlsbad, California,
United States of America

ABSTRACT. A one-dimensional, steady-state, relativistic Fokker–Planck model of electron cyclotron heating (ECH) is used to analyse the heating kinetics underlying the formation of the two-component hot-electron plasmas characteristic of ECH in magnetic mirror configurations. The model is first applied to the well diagnosed plasmas obtained in SM-1 and is then used to simulate the effective generation of relativistic electrons by upper off-resonant heating (UORH), as demonstrated empirically in ELMO. The characteristics of unstable whistler modes and cyclotron maser modes are then determined for two-component hot-electron plasmas sustained by UORH. Cyclotron maser modes are shown to be strongly suppressed by the colder background electron species, while the growth rates of whistler modes are reduced by relativistic effects to levels that may render them unobservable, provided the hot-electron pressure anisotropy is below an energy dependent threshold.

1. INTRODUCTION

Early experiments on electron cyclotron heating (ECH) of plasmas confined in magnetic mirrors [1] using CW microwave power at a single frequency created an unusual plasma containing two distinct populations of electrons. The majority of the electrons remained at a temperature that was typically below 100 eV, while a small fraction was heated to average energies above 100 keV. Rather broad regimes of stable operation were found to be limited by the onset of several dominant modes of instability, such as the mirror mode, the flute mode and unstable whistler waves. Later experiments in the ELMO facility [2] showed that the energy stored in the hot-electron component could be greatly increased by using upper off-resonant heating (UORH), in which microwave power at a frequency above the cold-electron gyrofrequency was added to the fundamental ECH power. In addition to increasing the relative density of the hot electrons, UORH also enhanced the stability of the plasma, even for values of beta in excess of 50% (beta is the conventional ratio of plasma kinetic pressure to magnetostatic pressure).

The stable, high-beta, hot-electron annulus revealed by the ELMO experiments led to the successful use of these plasmas ('ELMO rings') to stabilize a scalar pressure core plasma confined in the ELMO Bumpy Torus device (see, for example, Ref. [3]); this stimulated widespread interest in the fundamental properties of these remarkable plasmas (see, for example, Ref. [4]). Recently proposed applications for these hot-electron plasmas include stabilization of localized modes in heliacs [5] and tokamaks [6], as well as energy storage for subsequent conversion to high-power microwave pulses.

It has required the efforts of many workers to evolve reasonably satisfactory theoretical models of the steady state equilibrium produced in ECH experiments. The basic characteristics of the interaction of individual electrons with microwave electric fields were derived very early (for a discussion of early theoretical work, see Ref. [7]) and useful formulas were obtained for the resulting heating rate under a wide range of conditions (for a description of later work, see Ref. [8]). Subsequent development of geometrical optics codes (see, for example, Ref. [9]) made it possible to describe the propagation and absorption of microwaves in specified plasma media. Progress was accelerated by the formulation of a relativistic Fokker–Planck theory of ECH by Bernstein and Baxter [10]. Hamasaki and co-workers [11] took moments of the Fokker–Planck equation, using trial distribution functions, in an attempt to predict the power required for formation of the ELMO rings. Other workers [12] developed numerical techniques for a direct solution of the Fokker–Planck

equation; these are now implemented in large computer codes [13]. Ultimately, these codes are expected to provide a detailed, self-consistent picture of high-beta hot-electron plasmas formed by ECH.

Nonetheless, there is an immediate need for a reduced model that can be used to search over the wide range of parameters characterizing an ECH experiment. It is not practical to carry out such search with two-dimensional Fokker-Planck codes; this would require broad, time consuming parameter searches to overcome the general lack of experimental measurements of such essential parameters as the strength of each RF electric field component present in the plasma. We have addressed this need by evolving a Fokker-Planck model for the steady state distribution of electrons in energy; this model includes in a heuristic way the phenomena that depend essentially on the electron orientation in a gyrotropic, two-dimensional velocity space. This model has been described in considerable detail in Ref. [14].

In order to model a complex physical situation in a relatively simple way, the power balance issues affecting the formation of a relativistic electron tail have been considered primarily and not the particle balance issues, except in so far as a significant associated energy loss occurs, as in the case of non-adiabatic scattering of high energy electrons into the loss cone. For a more detailed justification of this approach, see the Appendix. Thus, we have chosen to conserve particles while accounting for the energy loss by converting the non-adiabatic loss term into a dynamical friction term, as described in Appendix C of Ref. [14]. This choice has the desired physical effect of sharply reducing the hot-electron distribution function for energies above the threshold for violation of adiabatic invariance, as is clearly evident in Figs 1a and 1b. The hot-electron distribution in energy is shown in Fig. 1a for plasmas typical of those reported in Ref. [15]. Figure 1b shows the four rates accounted for in the model: the quasi-linear heating rate, the Coulomb thermalization rate, the synchrotron radiation cooling rate and the energy loss rate due to non-adiabatic scattering.

Here, we first apply this reduced model to the SM-1 experiments [15] in order to demonstrate the success of this model in describing the hot-electron plasmas studied in SM-1. The results of this demonstration are presented and discussed in Section 2. They clarify a number of features of ECH experiments that had not been fully understood previously. In particular, the role of microwave electric fields parallel to the static magnetic field (ordinary mode of propagation) is

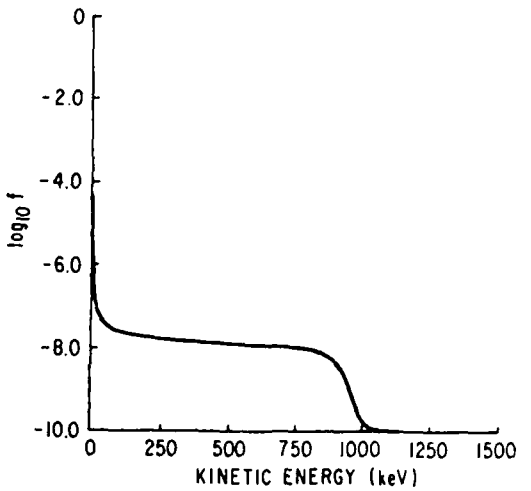

FIG. 1a. Electron distribution in energy for a case typical of the single-frequency heating experiments reported in Ref. [15].

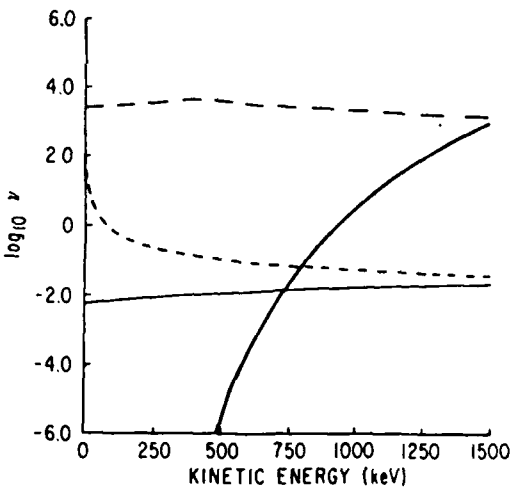

FIG. 1b. Characteristic rates entering into the heating kinetics (from top): electron heating rate due to ECH power; electron thermalization by Coulomb collisions with colder electrons; synchrotron radiation; and energy loss by non-adiabatic scattering of hot electrons into the loss cone.

shown to be critical to an effective formation of the hot-electron component. Furthermore, by exploiting the sensitivity of the hot-electron heating rate to the parallel microwave electric fields, we are able to use the reduced Fokker-Planck ECH model to demonstrate the impact of non-adiabatic scattering [16], which has been conjectured for some time to limit the maximum temperature of the hot electrons in most ECH experiments to date.

We then apply the present model to the UORH experiments in ELMO [2], where the model displays the same striking increases in stored energy with increasing UORH power that were observed in ELMO. Finally, the model is used to obtain high-beta hot-electron equilibria suitable for subsequent stability studies. Although the reduced model cannot provide information on pressure anisotropies or other two-dimensional properties of the equilibria, it does relate the relative temperatures and densities of the two electron species and provides a much larger degree of internal consistency than was heretofore available.

In Section 3, we analyse the stability of the hot-electron plasmas to transverse waves propagating along the static magnetic field, namely whistler waves [17] and the cyclotron maser modes (see, for example, Ref. [18a] and the excellent set of references cited therein; for more recent results, see Ref. [18b]). It has been known for many years [19] that relativistic effects generally reduce the growth rates of unstable whistler waves, but specific results depend on the assumed equilibrium. Here we use the Fokker–Planck model to obtain equilibria that are consistent with ECH kinetics and demonstrate the relativistic suppression of whistler growth rates. The cyclotron maser modes are found to be completely stabilized by the cold-electron component.

Finally, we note in passing that our understanding of flute modes in high-beta hot-electron plasmas has not been considered here and remains incomplete, although fully electromagnetic kinetic models of line tying [20] have helped clarify finite-length effects. There is an active effort to predict the stability of these high-beta plasmas to flute-like modes [21] which we hope will be aided by more detailed descriptions of realistic equilibria. Discussion and conclusions are found in Section 4.

2. FORMATION OF HOT-ELECTRON PLASMAS USING ECH

In this section we describe the results of applying the reduced Fokker–Planck ECH model to ECH experiments in the mirror devices SM-1 [15] and ELMO [2] before using the model to obtain high-beta equilibria for stability analysis. The Fokker–Planck model is described in great detail in Ref. [14] and references cited there.

Briefly, we use a one-dimensional, steady-state, bounce-averaged Fokker–Planck model of the ECH process. Since our primary concern is with the thermalization of a relatively small concentration of energetic electrons, we adopt a linearized, test-particle framework. The relativistic ('hot') electrons are then regarded as a distinct species whose spatial density n_h is much smaller than the densities of the other plasma species. All of these 'field' species are assumed to be isotropic, thermal, and at a much lower temperature than the hot electrons. This model determines the response of a small relative-density, high-energy electron tail to the incident microwave power by including the dominant dynamical processes: quasi-linear heating, thermalization by Coulomb scattering on cooler electrons, synchrotron radiation, and direct loss by non-adiabatic scattering. Specifically, the model predicts the electron distribution in energy resulting from RF electric fields with specified values of frequency, amplitude and polarization, incident upon a background plasma of specified density and temperature, confined in a prescribed mirror-like magnetic field.

TABLE I. SM-1 REFERENCE CASE (Ref. [15])

Stored energy	$W_\perp \approx 20$ J
Radius of annulus	$r_0 = 10.4$ cm
Radial width	$2\Delta = 5.8$ cm
Axial length	$L/2 = 12$ and 18 cm
Annulus volume	Vol $\approx 12 \times 10^3$ cm^3
Mirror ratio on axis	$M_0 = 2.2$
Coil separation	$L_c = 71$ cm
Mirror ratio at r_0	$M = 3$
Mirror ratio at resonance	$M_{res} = 2$
ECH power	$P \approx 1$ kW
Microwave frequency	$f \approx 9.5$ GHz
Background plasma	
density	$n \approx (1\text{-}3) \times 10^{11}$ cm^{-3}
temperature	$T_c \approx 10\text{-}50$ eV
Hot-electron component	
density	$n_h \approx 3 \times 10^{7}$ cm^{-3}
temperature	$T_h \approx 350\text{-}400$ keV

We take as our SM-1 reference case the 20 J equilibrium discussed at length in Ref. [15] and summarized in Table I. As mentioned earlier, there are no direct measurements of the strength of the microwave electric fields, and we must scan over all plausible values of both components, E_- and E_+. We do this by specifying the ratio E_+/E_- of the O-mode and X-mode field strengths and searching out the values of

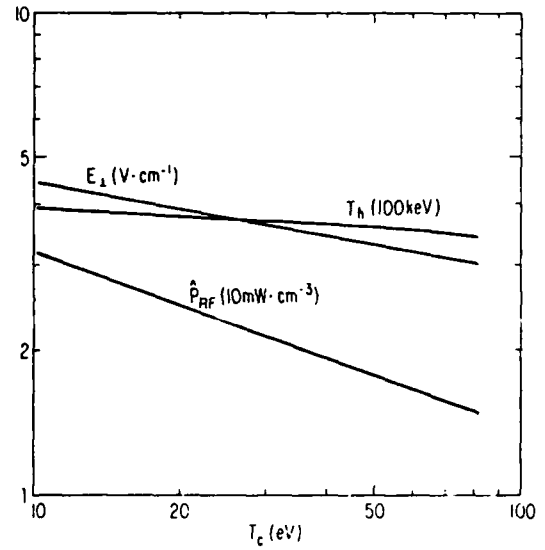

FIG. 2a. Perpendicular component of the microwave electric field, $E_\perp$, average energy of the hot electrons, T_h, and total RF power density, $\hat{P}_{RF}$, versus background plasma temperature, T_c, for an assumed ratio of O-mode to X-mode field strengths, $E_\parallel/E_\perp = 2$, in the SM-1 configuration summarized in Table I. The relative hot-electron density is $n_h/n = 0.1$.

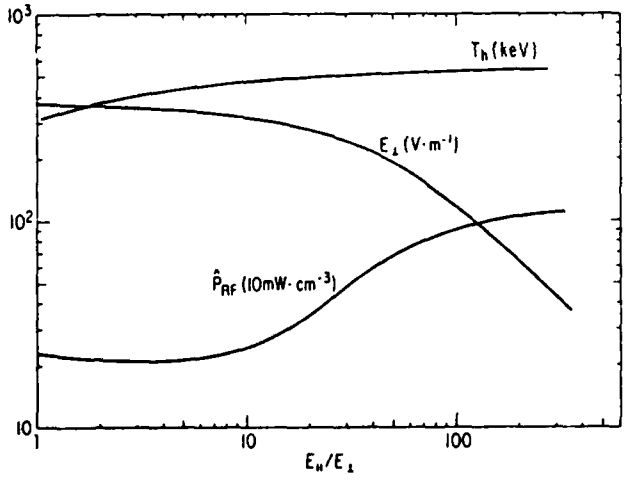

FIG. 2b. Variation of $E_\perp$, T_h and RF power density $\hat{P}_{RF}$ with $E_\parallel/E_\perp$ for a background plasma temperature $T_c = 30$ eV and $n_h/n = 0.1$.

$E_\perp$ required to sustain the observed relative hot-electron density, $n_h/n = 0.1$; this yields the observed hot-electron average energy T_h and the RF power density $\hat{P}_{RF}$ required to sustain the equilibrium. Since the microwave power is launched primarily in ordinary modes and is multiply reflected from the cavity walls, we assume an essentially isotropic distribution of wave vectors $\vec{k}$ for the ECH waves. An illustrative case is shown in Fig. 2a, which displays $E_\perp$, T_h and $\hat{P}_{RF}$ versus the background electron temperature T_c for $E_\parallel/E_\perp = 2$. The characteristic scale length of the static magnetic field has been set at $L_\parallel = 30$ cm for this case, a choice that we will discuss at length in the following. Note that the RF power density required to sustain this equilibrium is around 20 mW·cm^{-3}, accounting for roughly 250 W of RF power. This does not include the fundamental ECH power necessary to sustain the background plasma. If the energy expended in creating each ion–electron pair is roughly 50 eV, we estimate this fundamental ECH power requirement at 25 mW·cm^{-3} for an ambient hydrogen gas pressure of 5×10^{-6} torr. Since the cold-plasma volume is estimated at 25 L in Ref. [15], as much as 625 W of fundamental ECH power may be required simply to sustain the background plasma and only 250 W may be required to sustain the hot-electron component. The variation of $E_\perp$, T_h and $\hat{P}_{RF}$ with the ratio $E_\parallel/E_\perp$ is shown in Fig. 2b for a background electron temperature $T_c = 30$ eV. Note the rapid rise in RF power density for $E_\parallel/E_\perp > 10$, in which $\hat{P}_{RF}$ increases five times while the average energy of the hot electrons remains almost constant. The saturation of T_h despite a substantial increase in RF power indicates the rapid increase in the non-adiabatic scattering rate. If these calculations are repeated for different values of the magnetic scale length $L_\parallel$, we obtain the striking results shown in Fig. 3a. It is especially instructive to display the $L_\parallel$ dependence of the saturated value of the hot-electron average energy and the corresponding values of the electron gyroradius:

$$\rho_{sat} = 1.7 \times 10^3 \text{ G·cm } \sqrt{\hat{\epsilon}(2 + \hat{\epsilon})}/B$$

where $\hat{\epsilon} = T_{h,sat}/m_0c^2$ and B is the magnetic intensity. Since we require $\rho \leq kL_\parallel$ for adiabatic confinement of electrons, we can evaluate k by plotting ρ_{sat} versus $L_\parallel$. The value of k obtained from Fig. 3b is 0.06, which agrees reasonably well with the conventional result cited by Uckan [16]. From the values obtained for $T_{h,sat}$ it appears that $L_\parallel = 24$ cm is a reasonable value of the magnetic scale length in the hot-electron region of SM-1. From a parabolic fit to the vacuum magnetic intensity we would estimate $L_\parallel = 21$ cm, in reasonable agreement. Note that this is much less than R_c, the radius of curvature of the magnetic field lines in this region, which is estimated to be around 60 cm.

For large values of $L_\parallel$, particularly at higher magnetic fields, synchrotron radiation becomes a dominant loss mechanism in the model. This loss is

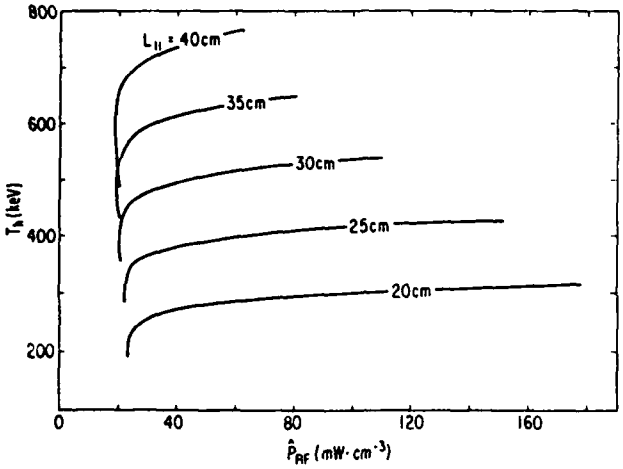

FIG. 3a. T_h versus $\hat{P}_{RF}$ for different values of the magnetic scale length $L_{||}$.

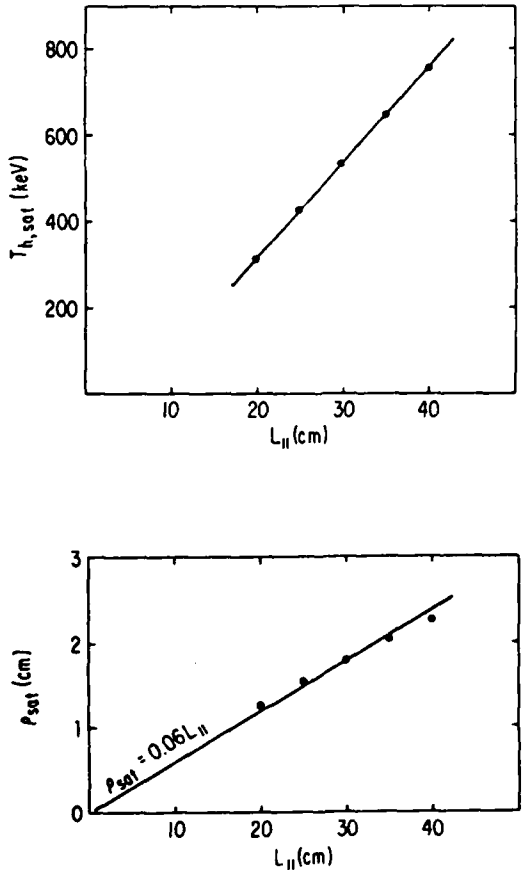

FIG. 3b. Saturated value of $T_{h,sat}$ and corresponding value of the average hot-electron gyroradius ρ_{sat} versus $L_{||}$. The solid line is for $\rho_{sat} = 0.06\ L_{||}$.

circumvented in the case discussed here by specifying values of $L_{||}$ similar to the ELMO (high field) experiments: $L_{||}$ = 10 cm (ELMO).

Another important feature of the dependence of T_h on $E_{||}/E_{\perp}$ is the rapid initial increse in T_h, with $\hat{P}_{RF}$ constant or even decreasing. This behaviour makes clear the substantial benefit of increased microwave integrity of the vacuum chamber. If $E_{||}/E_{\perp} \geq 10$ can be sustained in a suitably designed cavity where wall reflections do not rapidly convert ordinary modes to extraordinary modes, T_h can be increased by roughly 100 keV or more. Since the value of $E_{||}$ required to achieve this level of heating is approximately 10^2 V·cm^{-1}, while the power density dissipated in the plasma is around 1 W·cm^{-3}, the effective quality factor must exceed 300. The ELMO device [2] utilized a very high-Q cavity together with UORH power to obtain exceptionally efficient heating of relativistic electrons. The frequency of the UORH power is chosen to be above the cold electron gyrofrequency throughout the entire cavity. This power is therefore absorbed primarily by the relativistic electrons and only negligibly by the background electrons. Even for the hot electrons, the absorption rate is small; thus, if the cavity has a large quality factor, the electric field strength can increase to large enough values to render the heating rate (and hence the absorption rate) appreciable. Since heating rates are quadratic in electric field strength, they can be large enough to sustain high energy electron populations at levels below 100 V·cm^{-1}.

The Fokker-Planck simulation of early ELMO experiments on UORH [2] are shown in Fig. 4. Here the fundamental ECH is at a frequency of 10.6 GHz while the UORH source has a frequency of 35.7 GHz. These results compare favourably with the empirical results displayed in Fig. 4 of Ref. [2]. The background plasma density and temperature are 2×10^{11} cm^{-3} and 50 eV, respectively, and we have arbitrarily set $E_{||}/E_{\perp}$ = 10 for both sources. In the absence of UORH power, the relative density of hot electrons is roughly 2.5%, sustained by an RF power density of less than 6 mW·cm^{-3}. This relative density increases to 64% and the hot-electron beta approaches 50% as the UORH power is increased.

Having calibrated our model on SM-1 and ELMO, it is of interest to see how much hot-electron energy can be stored in comparably sized devices by optimizing the parameters. By using UORH at higher frequencies (60/90 GHz) in a device that is similar in physical scale to ELMO, we can obtain Fokker-Planck equilibria with average hot-electron energies above

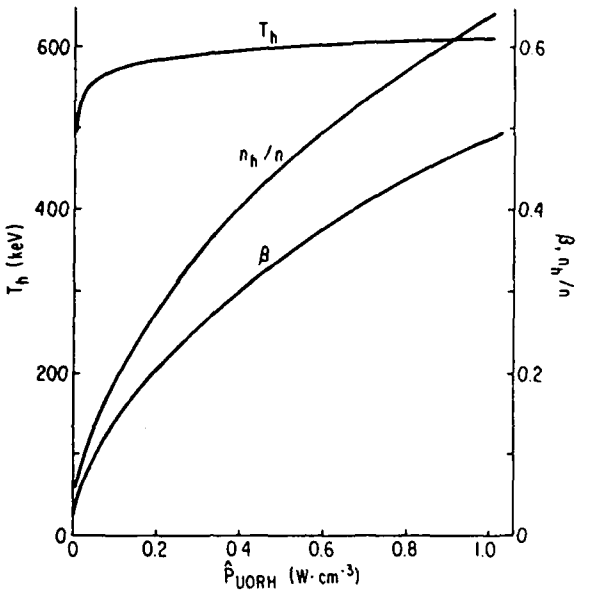

FIG. 4. Average hot-electron energy, T_h, relative hot-electron density, n_h/n, and plasma beta, β, versus power density from the UORH source, $\hat{P}_{UORH}$. The parameters describing the background plasma and the heating configuration are given in the text.

m_0c^2. The relativistic effects on plasma stability can be clearly examined in this hot-electron temperature range. In these studies, we have again specified the background plasma density at $n = 1 \times 10^{13}$ cm^{-3} and varied the background electron temperature T_c from 250 to 3000 eV. We assume that optimal background electron temperatures can be maintained by a suitable level of fundamental ECH power, depending mainly on the confinement properties of the configuration. For the Fokker-Planck model of the hot-electron population we reduce the fundamental ECH electric field strength to a negligible level: 10^{-3} times the UORH field strength. We then vary T_c over its range to determine the values of UORH power density $\hat{P}_{RF}$ required to sustain specified relative densities of hot electrons. The Fokker-Planck model evaluates T_h for specified values of the various system parameters, such as the magnetic field scale length L_I, here set at 10 cm, as in ELMO. These results are displayed in Fig. 5. Note that, since these curves are deduced for constant hot-electron densities $\Delta_h = n_h/n$, the resulting value of beta is simply porportional to T_h. The RF power density exhibits a broad minimum that moves from 500 eV to 800 eV as the hot-electron density ratio is increased from 10% to 40%. The associated beta values approach 50% and the hot-electron average energy is around 550 keV. These are the equilibria whose stability will be studied in the following sections.

3. STABILITY ANALYSIS FOR TRANSVERSE WAVES PROPAGATING PARALLEL TO THE STATIC MAGNETIC FIELD

As discussed in Section 2, the first task addressed in this work was to obtain high-beta equilibria from the reduced one-dimensional Fokker-Planck model of the ECH process. Guided by the empirical results of Dandl et al. [2] on UORH in the ELMO experiments, we found a corresponding regime in the Fokker-Planck analysis that yields high-beta, relativistic-electron equilibria ideally suited to a stability analysis, namely beta values around 50% and relativistic-electron temperatures above 500 keV. Our one-dimensional Fokker-Planck model cannot provide any information on the temperature anisotropy that is characteristic of hot-electron plasmas formed by ECH and which plays a dominant role in the stability of these plasmas [22]. Fully two-dimensional Fokker-Planck ECH codes are now available and will eventually provide two-dimensional equilibria. These numerical equilibria can be expressed analytically as a superposition of the equilibrium distribution functions described by Guest and Dory [23]:

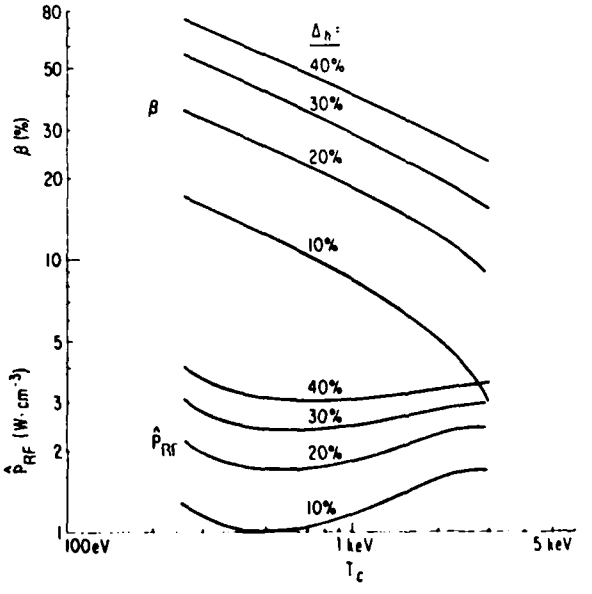

FIG. 5. RF power density required and beta values achieved in maintaining specified values of relative hot-electron density versus background electron temperature T_c. The background plasma density is 10^{13} cm^{-3} and the ECH frequencies are 60 and 90 GHz.

$$f^{(0)}(u_\perp^2, u_\parallel^2) = \frac{n}{\pi^{3/2}\alpha_\perp^2\alpha_\parallel \ell!}\left[\frac{u_\perp}{\alpha_\perp}\right]^{2\ell} \times \exp\left[-\frac{u_\perp^2}{\alpha_\perp^2} - \frac{u_\parallel^2}{\alpha_\parallel^2}\right]$$

where $\ell = 0, 1, 2, \ldots$, and $\vec{u} = \vec{p}/m$ is the momentum per unit rest mass. Here, we examine our one-dimensional equilibria for stability against transverse waves propagating parallel to the static magnetic field, with the temperature anisotropy $\eta \equiv T_\perp/T_\parallel$ and the loss-cone index ℓ set at arbitrary values. We single out the whistler mode [17, 19, 24] and the cyclotron maser mode [18, 24] because of the relative stringency of the stability criteria for electrostatic and whistler modes, as discussed by Guest and Sigmar [22], and because the cyclotron maser mode was omitted from consideration in Ref. [22].

In what follows, we describe an efficient and very rapid numerical technique for solving the fully relativistic dispersion relation for right-hand, circularly polarized, transverse waves propagating parallel to the equilibrium magnetic field. The derivation of the dispersion relation is sketched here for completeness; more detailed discussions are readily available [25].

The relativistic Vlasov equation for electrons is

$$(\partial f/\partial t) + (\vec{u}/\gamma)(\partial f/\partial \vec{r}) - (e/m)[\vec{E} + (\vec{u} \times \vec{B})/\gamma](\partial f/\partial \vec{u}) = 0$$

where $\gamma^2 = 1 + u^2/c^2$ is the Lorentz factor and the velocity is $\vec{v} = \vec{u}/\gamma$. The perturbed distribution function, associated with a wave whose electric and magnetic fields are $\vec{E}$ and $\vec{B} = \vec{k} \times \vec{E}/\omega$, is given by

$$f_1(\vec{r}, \vec{u}, t) = \frac{e}{m}\int_{-\infty}^{t} dt' \times \left[\left(1 - \frac{\vec{k}\cdot\vec{u}}{\gamma\omega}\right)\vec{E}\cdot\frac{\partial f_0}{\partial \vec{u}} + \frac{\vec{u}\cdot\vec{E}}{\gamma\omega}\,\vec{k}\cdot\frac{\partial f_0}{\partial \vec{u}}\right]$$

For purely transverse waves propagating parallel to the equilibrium magnetic field, with components $E_\pm = (E_x \pm iE_y)/\sqrt{2}$, this expression becomes

$$f_1(\vec{r}, \vec{u}, t) = \sqrt{2}\,\frac{e}{m}\int_{-\infty}^{t} dt' \times \left[\left(1 - \frac{ku_\parallel}{\gamma\omega}\right)\frac{\partial f_0}{\partial u_\perp^2} + \frac{ku_\parallel}{\gamma\omega}\,\frac{\partial f_0}{\partial u_\parallel^2}\right] \times u_\perp(E_+e^{-i\phi} + E_-e^{i\phi})$$

where ϕ is the polar angle. In the uniform magnetic field assumed here, the unperturbed electron orbits are given by $z = z_0 + u_\parallel t/\gamma$ and $\phi = \phi_0 + eBt/\gamma m$, with $u_\parallel$ and $u_\perp$ constant. Choosing $z_0 = 0$ at $t = 0$, we obtain

$$f_1(z=0, \vec{u}, t=0) = -i\sqrt{2}u_\perp(e/m) \times \left[\left(\gamma - \frac{ku_\parallel}{\omega}\right)\frac{\partial f_0}{\partial u_\perp^2} + \frac{ku_\parallel}{\omega}\,\frac{\partial f_0}{\partial u_\parallel^2}\right] \times \left(\frac{E_+e^{-i\phi}}{ku_\parallel - \gamma\omega - eB/m} + \frac{E_-e^{i\phi}}{ku_\parallel - \gamma\omega + eB/m}\right)$$

From Faraday's and Ampere's laws,

$$\nabla \times (\nabla \times \vec{E}) = -\mu_0(\partial/\partial t)[\vec{j} + \epsilon_0(\partial\vec{E}/\partial t)]$$

or

$$k^2\vec{E} - (\vec{k}\cdot\vec{E})\vec{k} - (\omega^2/c^2)\vec{E} = i\omega\mu_0\vec{j}$$

Since $\vec{k}\cdot\vec{E} = 0$ for transverse waves, $\vec{E}$ and $\vec{j}$ must satisfy

$$[(k^2c^2/\omega^2) - 1]\vec{E} = (i/\omega\epsilon_0)\vec{j}$$

For the right-hand, circularly polarized component, the resulting dispersion relation is

$$\frac{k^2c^2}{\omega^2} - 1 = \frac{-e^2}{m\omega\epsilon_0}\,2\pi\int_0^\infty u_\perp^3\,du_\perp\int_{-\infty}^{\infty} du_\parallel \times \frac{\left(1 - \frac{ku_\parallel}{\gamma\omega}\right)\frac{\partial f_0}{\partial u_\perp^2} + \frac{ku_\parallel}{\gamma\omega}\,\frac{\partial f_0}{\partial u_\parallel^2}}{ku_\parallel - \gamma\omega + eB/m}$$

For the class of equilibrium distribution functions discussed by Guest and Dory [23], the numerator of the integrand can be rewritten conveniently as

$$\left(1 - \frac{ku_\parallel}{\gamma\omega}\right)\frac{\partial f_0}{\partial u_\perp^2} + \frac{ku_\parallel}{\gamma\omega}\frac{\partial f_0}{\partial u_\parallel^2}$$

$$= \frac{f_0}{\alpha_\perp^2}\left[\frac{ku_\parallel}{\gamma\omega}\left(1 - \frac{\ell\alpha_\perp^2}{u_\perp^2} - \frac{\alpha_\perp^2}{\alpha_\parallel^2}\right)\right.$$

$$\left. - \left(1 - \frac{\ell\alpha_\perp^2}{u_\perp^2}\right)\right]$$

Since the Lorentz factor γ appears in the resonant denominator and since we are concerned with strongly relativistic plasmas with $\gamma \gtrsim 2$, it is necessary to evaluate the integral numerically. We now consider integrals of the general form

$$I(\omega, k) = \int_0^\infty du_\perp^2\, e^{-u_\perp^2/\alpha_\perp^2} \int_{-\infty}^{\infty} du_\parallel\, e^{-u_\parallel^2/\alpha_\parallel^2} \times \frac{F(u_\parallel, u_\perp^2, \omega, k)}{ku_\parallel - \gamma\omega + eB/m}$$

For complex values of ω and k, there may be zero, one or two solutions to the relativistic resonance condition $ku_\parallel - \gamma\omega + eB/m$, which we denote by $u_{\parallel i}$ ($i = 1, 2$). We denote each solution for $u_\parallel(\omega, k, u_\perp^2)$ by w and the corresponding values of γ by $\gamma_i^2 = \sqrt{1 + w_i^2/c^2 + u_\perp^2/c^2}$. Now consider the following integral:

$$\int_{-\infty}^{\infty} du_\parallel\, e^{-u_\parallel^2/\alpha_\parallel^2} \frac{F(w_i, u_\perp^2, \omega, k)}{ku_\parallel - \gamma_i\omega + eB/m}$$

$$= \alpha_\parallel F(w_i, u_\perp^2, \omega, k) \int_{-\infty}^{\infty} dy\, \frac{e^{-y^2}}{k\alpha_\parallel y - \gamma_i\omega + eB/m}$$

$$= \frac{\sqrt{\pi}}{k} Z\left(\frac{\gamma_i\omega - eB/m}{k\alpha_\parallel}\right) F(w_i, u_\perp^2, \omega, k)$$

for $\quad \mathrm{Im}\left(\dfrac{\gamma_i\omega - eB/m}{k\alpha_\parallel}\right) > 0$

where Z is the conventional plasma dispersion function [26]. From this, we obtain:

$$I(\omega, k) = \int_0^\infty du_\perp^2\, e^{-u_\perp^2/\alpha_\perp^2} \frac{\sqrt{\pi}}{k} Z\left(\frac{\gamma_i\omega - eB/m}{k\alpha_\parallel}\right) \times F(w_i, u_\perp^2, \omega, k) + \int_0^\infty du_\perp^2\, e^{-u_\perp^2/\alpha_\perp^2} \int_{-\infty}^{\infty} du_\parallel\, e^{-u_\parallel^2/\alpha_\parallel^2} \times \left(\frac{F(u_\parallel, u_\perp^2, \omega, k)}{ku_\parallel - \gamma\omega + eB/m} - \frac{F(w_i, u_\perp^2, \omega, k)}{ku_\parallel - \gamma_i\omega + eB/m}\right)$$

With the singularities removed in this manner, the $u_\parallel$ integral can be evaluated using the Gauss-Hermite quadrature [27]:

$$\int_{-\infty}^{\infty} du_\parallel\, e^{-u_\parallel^2/\alpha_\parallel^2} \Xi(u_\parallel) = \sum_{i=1}^{s} W_{H,i}\, \Xi(u_{\parallel,i})$$

Similarly, the $u_\perp$ integral can be evaluated using the Gauss-Laguerre quadrature [26]

$$\int_0^\infty du_\perp^2\, e^{-u_\perp^2/\alpha_\perp^2} \Psi(u_\perp^2) = \sum_{i=1}^{s} W_{L,i} \Psi(u_{\perp,i}^2)$$

To evaluate the dispersion relation for given values of ω and k, we then choose a value of s ($s = 12$ typically) and for each of the s prescribed values of $u_{\perp,i}^2$ ($i = 1, \ldots, s$) we evaluate the corresponding root or roots of the relativistic resonance condition, $u_{\parallel,i} = w_i$, such that

$$k_r w_i - \hat{\gamma}_i\omega_r + eB/m = 0$$

The Gauss-Hermite formula is then used to calculate

$$G(\omega, k, u_{\perp,i}^2) \equiv \int_{-\infty}^{\infty} du_\parallel\, e^{-u_\parallel^2/\alpha_\parallel^2} \times \left(\frac{F(u_\parallel, u_{\perp,i}^2, \omega, k)}{ku_\parallel - \omega\sqrt{(1 + (u_\parallel^2/c^2) + (u_{\perp,i}^2/c^2))} + eB/m} - \frac{F(w_i, u_{\perp,i}^2, \omega, k)}{ku_\parallel - \omega\sqrt{(1 + (w_i^2/c^2) + (u_{\perp,i}^2/c^2))} + eB/m}\right)$$

$$= \sum_{j=1}^{s} W_{H,j}\, \Xi_i(u_{\parallel,j}, u_{\perp,i}^2, \omega, k)$$

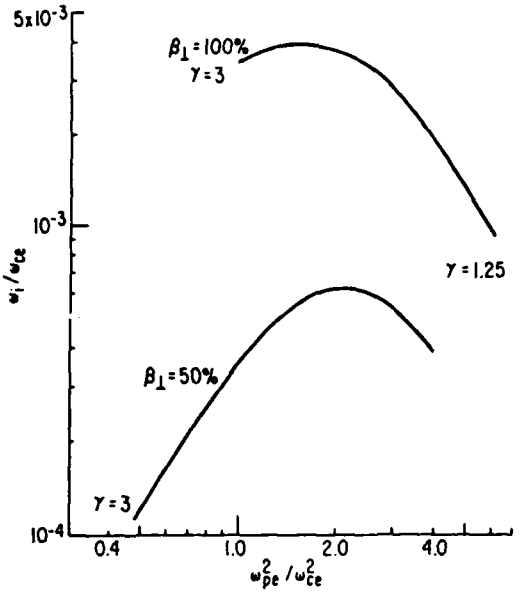

FIG. 6. Density dependence of cyclotron maser mode growth rate for fixed values of beta. The plasma parameters are specified in the text.

A standard routine is used to evaluate the plasma dispersion function, and the Gauss–Laguerre quadrature is used to evaluate the $u_\perp^2$ integral:

$$I(\omega, k) = \int_0^\infty du_\perp^2 \, e^{-u_\perp^2/\alpha^2}$$

$$\times \left[\frac{\sqrt{\pi}}{k} Z\left(\frac{\hat{\gamma}\omega - eB/m}{k\alpha_\parallel} \right) F(w_i, u_\perp^2, \omega, k) \right.$$

$$\left. + G(\omega, k, u_\perp^2) \right] = \sum_{p=1}^{s} W_{L,p} \, \Xi_2(u_{\perp,p}^2, \omega, k)$$

With this algorithm for evaluating the velocity-space integrals, we can use standard root-finding routines to solve the dispersion relation for fully relativistic hot-electron plasmas. In this way we can evaluate the threshold conditions and growth rates for unstable whistler and cyclotron maser modes in the high-beta hot-electron plasmas obtained from our Fokker–Planck model. As has been pointed out by Chu and Hirshfield [18a], whistler waves with phase velocities below the speed of light are destabilized by the temperature anisotropy, while the cyclotron maser mode, corresponding to waves with phase velocities greater than the speed of light, are destabilized by the beam-like/loss-cone aspect of the mirror-confined relativistic-electron equilibria [28]. Of particular interest for the present studies is the stabilizing effect of a cold-electron component on the cyclotron maser mode. Since our Fokker–Planck ECH equilibria consist of a minority population of relativistic electrons in a majority population of much colder background electrons, cyclotron maser modes are anticipated to be strongly suppressed. This is illustrated in the results shown in Fig. 6, where we fix the beta value at 50% and 100%, and the relative density of hot electrons at 30%. The hot-electron distribution has a loss cone index $\ell = 2$, and a temperature anisotropy $\eta \equiv T_\perp/T_\parallel = 3$. The peak temporal growth rate ω_i normalized by the (non-relativistic) electron gyrofrequency ω_{ce} is plotted against the total electron density, specified through the ratio of electron plasma and gyrofrequencies, $(\omega_{pe}/\omega_{ce})^2$. For the parameters of interest, the peak growth rates are less than 10^{-3} times the gyrofrequency. Figures 7a and 7b demonstrate the fundamental dependence of the cyclotron maser modes on the loss-cone index ℓ, rather than the temperature anisotropy. For these cases, the hot-electron beta is fixed at 30%, the total density at $\omega_{pe}^2 = \omega_{ce}^2/2$, and the relative density of hot electrons at 50%.

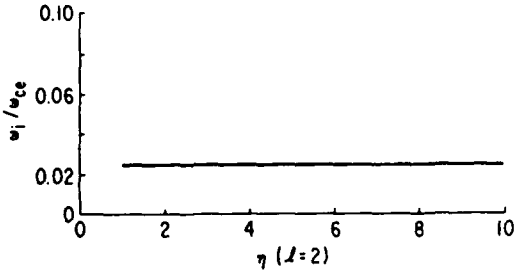

FIG. 7a. Demonstration of the independence of the cyclotron maser mode growth rate with respect to temperature anisotropy.

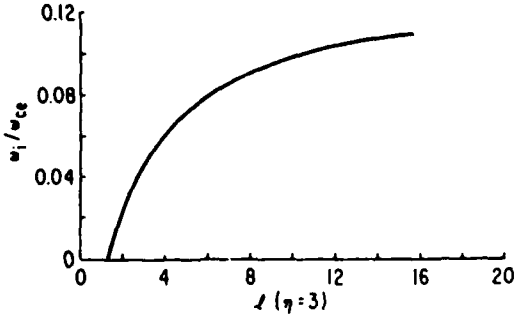

FIG. 7b. Dependence of the cyclotron maser mode growth rate on the loss-cone index ℓ.

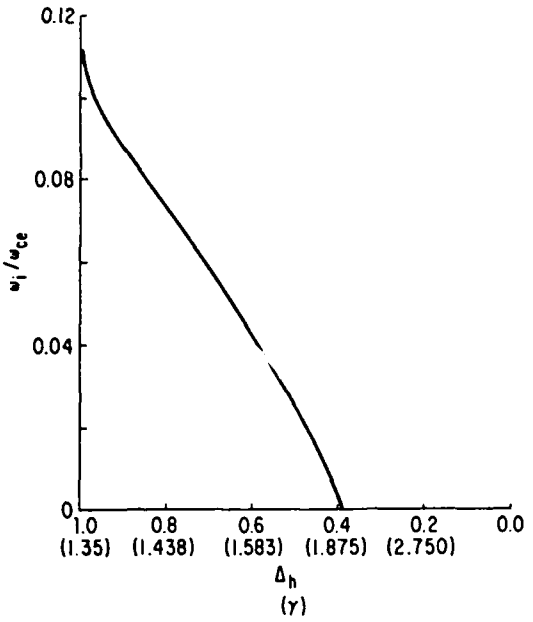

FIG. 8. Stabilization of the cyclotron maser mode by background cold electrons. The relative density of hot electrons is $\Delta_h = n_h/n$.

Finally, Fig. 8 shows how the growth is suppressed by decreasing the relative density of hot electrons, Δ_h. In this particular case, stabilization is complete for $\Delta_h \lesssim 40\%$; here, $\beta = 30\%$ and $\omega_{pe}^2/\omega_{ce}^2 = 0.5$. Tsang [24] considered this effect, but only for large values of Δ_h where he did not see complete stabilization.

By comparison, the whistler waves can have growth rates that are larger by two orders of magnitude if the anisotropy exceeds a critical value, which is about three for parameters characteristic of hot-electron plasmas formed by ECH. Indeed, whistler growth rates can be reduced to low values mainly by increasing the average energy of the hot electrons and decreasing the temperature anisotropy. These two effects are illustrated in Figs 9a and 9b, in a single-species hot-electron plasma with $\ell = 0$, $\eta = 3$ and $\beta = 30\%$. The average perpendicular energy is expressed as $\epsilon_\perp = T_h/mc^2$; in Fig. 9b, $\epsilon_\perp = 1$. Finally, we evaluate the whistler growth rates in a two-component equilibrium obtained from the Fokker-Planck ECH model: $T_h = 527$ keV, $\Delta_h = 30\%$, $T_c = 800$ eV, $\omega_{pe}^2/\omega_{ce}^2 = 0.5$ and $\beta = 31\%$. The temperature anisotropy has been varied ($\eta = 3, 6, 10, 20$) to show the rapid decrease in growth rate for decreasing anisotropy, as displayed in Fig. 10a. For the weakly unstable whistler waves the growth is convective. It is thus of interest to evaluate the spatial amplification rates k_i, as illustrated in Fig. 10b.

4. DISCUSSION AND CONCLUSIONS

We have demonstrated several points in this paper. First of all, using the classical Fokker-Planck model of ECH, it is possible to reproduce all of the features of the SM-1 experimental results that can be compared with the reduced one-dimensional model. In particular, there is no need to invoke collective processes, such as

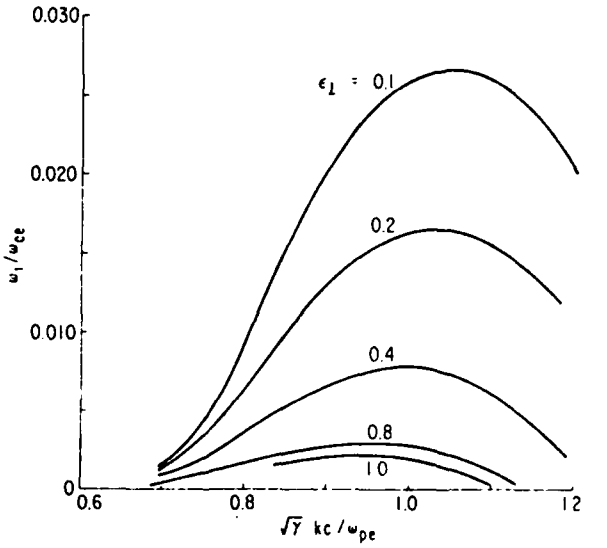

FIG. 9a. Whistler mode growth rates for fixed anisotropy, $\eta = 3$, and different values of the average hot-electron energy. The plasma parameters are specified in the text.

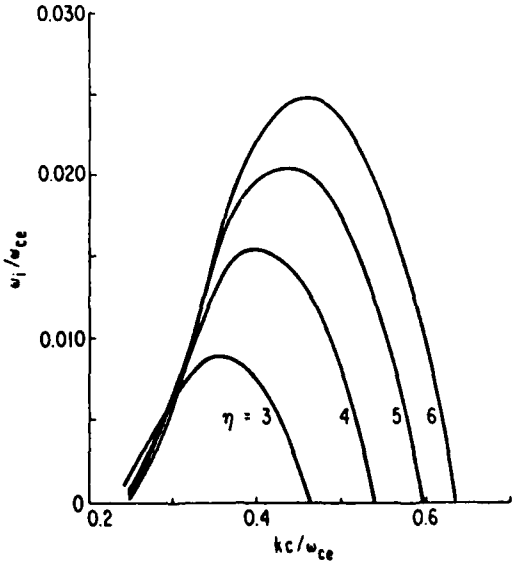

FIG. 9b. Whistler mode growth rates for fixed average hot-electron energy, $\epsilon_\perp = 1$, and different values of the temperature anisotropy.

unstable whistler waves, to provide a self-consistent picture of the hot-electron distribution in energy and the RF power density required to sustain it. This property of the present Fokker–Planck model is in contrast to the moment approach of Hamasaki et al. [11], as one might expect from the non-Maxwellian character of the hot-electron equilibrium distribution. An interesting possibility is suggested by these results, namely that a different class of test distribution functions, similar to those obtained here, could be used in the moment approach to obtain useful analytic descriptions of ECH equilibria.

The numerical description obtained in the present work also contributes to clarifying the role of non-adiabatic scattering in limiting the hot-electron energy and it reveals in quantitative terms the importance of the microwave integrity of the cavity in which the ECH is carried out. For single-frequency heating it is apparently necessary to have a high enough cavity quality factor to permit the ordinary mode field strength to exceed by a large factor the extraordinary mode electric field strength. Similarly, UORH can only be expected to yield the high energy densities observed in ELMO if the UORH field strengths can approach values of the order of 10^2 V·cm^{-1}, while the corresponding absorbed power densities remain around 1 W·cm^{-3} or less.

These results are of practical importance in designing experimental ECH approaches to achieving relativistic-electron plasmas; but they also suggest that the reduced Fokker–Planck model can provide a useful simplified description of other plasmas in which ECH may occur, such as magnetospheric plasmas.

For our immediate purposes, the reduced Fokker–Planck model provides a detailed, self-consistent description of hot-electron plasmas that can be analysed for stability. In keeping with a large body of empirical observations, we find that whistler waves are likely to be unstable unless the temperature anisotropy is reduced and the hot-electron energy is increased. Cyclotron maser modes are shown to be suppressed by the cold background electrons that normally make up the majority species in an ECH plasma.

In a recent PhD thesis, Garner [29] has studied the characteristics of microinstabilities in an ECH plasma produced in a magnetic well configuration by single-frequency heating. Garner finds that the hot-electron component, whose temperature is 400 keV, is remarkably stable; the observed unstable whistler waves are apparently driven by a distinct group of warm electrons at a temperature around 2 keV. The third electron component is a cold population at a temperature

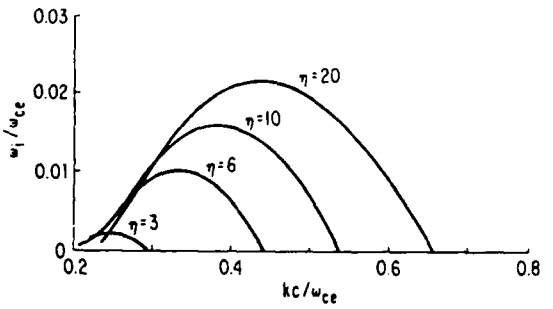

FIG. 10a. Whistler mode temporal growth rates for a Fokker–Planck ECH equilibrium with ad hoc values of the temperature anisotropy.

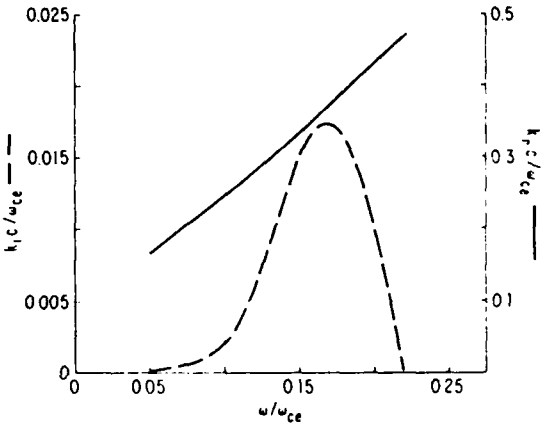

FIG. 10b. Whistler mode spatial growth rates and propagation vector for the Fokker–Planck ECH equilibrium with $\eta = 3$.

around 100 eV. The cold-, warm- and hot-electron densities are roughly equal and are in the range of $(1\text{–}2) \times 10^{11}$ cm^{-3}. Garner's thesis contains an interesting speculation regarding the observed stability of the hot-electron group that is not predicted by his analyses, namely that, if stochastic heating can occur at energies above the predicted threshold for super-adiabatic electron behaviour, the resulting distribution of hot electrons might indeed be stable at high temperatures. Our kinetic model of the relativistic heating process assumes that stochastic heating is maintained by the overlap of relativistic, Doppler-shifted resonances, and our analysis of the resulting equilibria demonstrates the relativistic stabilization of whistler waves as well as the cold-electron stabilization of the fast-wave branch of the electromagnetic mode. The distinct warm-electron component can be minimized or even eliminated by the use of O-mode heating or UORH, as shown by the present Fokker–Planck results.

APPENDIX

In brief, our picture of particle balance in mirror-confined ECH plasmas is as follows:

A-1. Low-energy processes

At energies $\epsilon \lesssim 100$ eV, particle balance is maintained by three dominant processes, namely (i) ionization of ambient neutral gas, (ii) free flow of cold ions along the magnetic lines of force and out the ends of the magnetic mirror, and (iii) electrostatic confinement of electrons in an ambipolar potential well whose depth Φ is governed by the electron heating rate $\dot{\epsilon}$ and the cold-ion escape rate.

Equating the ion and electron confinement times yields

$$e\Phi \simeq L\dot{\epsilon}/v_i$$

where v_i is the cold-ion flow velocity and L is the length of the plasma column. Furthermore, the escape of these electrons and cold ions is balanced by ionization, so that

$$v_i/L \simeq n_0\langle\sigma_{\text{ionization}}v_e\rangle$$

where n_0 is the density of neutral gas in the plasma. Under typical conditions, the characteristic rates for these three processes are around $5 \times 10^4\ s^{-1}$.

A-2. Intermediate-energy processess

In the energy range 100 eV $\lesssim \epsilon \lesssim$ 10 keV, the dominant dynamical processes are Coulomb scattering and ECH. The Coulomb scattering causes both slowing-down and pitch-angle scattering of heated electrons. For energy balance, the slowing-down must be offset by ECH for energies above a relatively low critical energy $\epsilon \gtrsim \epsilon_1 \approx 3e\Phi$:

$$|\dot{\epsilon}_{RF}(\epsilon_1)| = |\dot{\epsilon}_{Coul}(\epsilon_1)|$$

Using rudimentary formulas for each rate, we obtain

$$\frac{\pi e E_{RF}^2}{2B_0 M_t}\left(\frac{M-1}{M_t-1}\right)^{1/2} K^{-1}\left(\frac{M_t-1}{M-1}\right) = \frac{n_e \ln\Lambda}{1.3\times 10^5\,\epsilon_1^{1/2}}\ \frac{eV^{3/2}\,cm^3}{s}$$

For typical values of the ECH electric field, $E_{RF} \approx 10$–$20\ V\cdot cm^{-1}$, the central magnetic field, $B_0 \approx 3$ kG, the electron density, $n_e \approx 5\times 10^{11}\ cm^{-3}$, the overall mirror ratio, $M \approx 2$, and the mirror ratio at the test electron turning point, $M_t \approx 1.7$, the critical electron energy for runaway, ϵ_1, can be just above 100 eV. (Here, K is the elliptic integral associated with the electron bounce motion.)

Simultaneously, with ECH, small-angle Coulomb collisions scatter heated electrons into the loss cone at a rate given by

$$\left(\frac{d\theta^2}{dt}\right) \simeq 1.5\times 10^{-6}\ \frac{n_e \ln\Lambda}{\epsilon^{3/2}}\ \frac{eV^{3/2}\,cm^3}{s}$$

The corresponding rate of pitch-angle diffusion associated with ECH is given by

$$\left(\frac{d\theta^2}{dt}\right)_{RF} \simeq \frac{\pi}{8}\frac{eE_{RF}^2}{B_0\epsilon}\left(\frac{M_t}{M_{res}}-1\right)^2 \times\left(\frac{M-1}{M_t-1}\right)^{1/2}\frac{K^{-1}\left(\frac{M_t-1}{M-1}\right)}{M_t(M_t-1)}$$

where M_{res} is the mirror ratio at the resonant surface. Since $\dot{\theta}_{RF} \propto \epsilon^{-1}$, while $\dot{\theta}_{Coul} \propto \epsilon^{-3/2}$, RF-driven pitch-angle diffusion may dominate at high energies, $\epsilon > \epsilon_2 \approx 10$ keV, typically. In the intermediate energy range, $\epsilon_1 \lesssim \epsilon \lesssim \epsilon_2$, Coulomb scattering is typically the dominant loss process. The resulting pitch-angle displacement of an electron with initial pitch angle θ_i can be estimated from

$$\Delta\theta \simeq \int_{\epsilon_1}^{\epsilon_2}\frac{\dot{\theta}_{Coul}}{\dot{\epsilon}_{RF}}\,d\epsilon$$

Since $\dot{\epsilon}_{RF}$ is almost independent of energy in this range, we have

$$\frac{\Delta\theta}{\theta_i} = \frac{1.5\times 10^{-6}\,n_e \ln\Lambda}{\theta_i^2\,\dot{\epsilon}_{RF}} \times\frac{eV^{3/2}\,cm^3}{s}\int_{\epsilon_1}^{\epsilon_2} d\epsilon\ \epsilon^{-3/2} = \frac{3\times 10^{-6}\,n_e \ln\Lambda}{\theta_i^2\,\dot{\epsilon}_{RF}}\left(\epsilon_1^{-1/2}-\epsilon_2^{-1/2}\right)\frac{eV^{3/2}\,cm^3}{s}$$

Typically, $(\Delta\theta/\theta_i) \ll 1$, provided the heating rate is sufficiently large, for example $\dot{\epsilon}_{RF} \leq 10^7$ eV·s^{-1}. Some of the runaway electrons will indeed be lost, especially for $\epsilon \gtrsim \epsilon_t$, but the fractional hot-electron density obtained from energy balance alone provides a useful estimate of an upper bound on this ratio. Note also that in the one-dimensional Fokker–Planck model we define the hot-electron density as consisting only of electrons with energies above a specified value, which is usually chosen as 20 keV. For $\epsilon > 20$ keV, the RF-driven pitch-angle diffusion typically exceeds pitch-angle scattering due to Coulomb collisions; the loss rate of heated electrons in this energy range is estimated to be very small. Since we specify the total electron density in the one-dimensional model and restrict the hot-electron component to those electrons for which Coulomb scattering is negligible, we expect the relative hot-electron density obtained from energy balance considerations to be a valid upper bound and a close estimate.

A-3. High-energy processes

In the energy range $\epsilon > 10$ keV, Coulomb scattering pitch-angle diffusion into the loss cone can typically be offset by RF-driven pitch-angle diffusion in which heated electrons diffuse *towards* the resonant surface (where $\omega_{RF} = NeB/\gamma m$, N = 1, 2, 3,...). Heating at the second and higher harmonics of the relativistic-electron gyrofrequency plays a major role in the maintenance of efficient stochastic heating and causes further pitch-angle diffusion towards the midplane of the magnetic mirror, $\theta = \pi/2$. Particle losses in this energy region are very small, and energy balance is dominated by relativistic ECH and synchrotron radiation up to the energy at which electrons cease to be adiabatic. The escape of a very small number of very high energy electrons has little effect on particle balance, but can completely offset continued heating to higher energies.

In summary, we suggest that the justification of separating energy balance and particle balance conditions rests on the smallness of $(\Delta\theta/\theta)$, as estimated above, as well as on the unusual nature of the RF-driven pitch-angle diffusion that tends to drive heated electrons back towards the resonant surface. We have attempted to minimize the impact of particle balance processes on our one-dimensional Fokker–Planck model by regarding only electrons with energies above 20 keV as 'hot electrons' and specifying the total density ab initio.

ACKNOWLEDGEMENT

This work was supported by the United States Air Force Office of Scientific Research, under Contract No. F49620-86-C-0055.

REFERENCES

[1] BECKER, M.C., DANDL, R.A., EASON, H.O., ENGLAND, A.C., KERR, R.J., ARD, W.B., Nucl. Fusion: 1962 Suppl., Part 1 (1962) 345.
ARD, W.B., DANDL, R.A., STETSON, R.F., Phys. Fluids **9** (1966) 1498.
[2] DANDL, R.A., EASON, H.O., EDMONDS, P.H., ENGLAND, A.C., Nucl. Fusion **11** (1971) 411.
[3] DANDL, R.A., GUEST, G.E., "The ELMO Bumpy Torus", Fusion, Vol. 1, Part B (TELLER, E., Ed.), Academic Press, New York (1981) 79.
[4] HOT-ELECTRON Ring Physics (Proc. 2nd Workshop San Diego, CA, 1981), Vols 1 and 2, CONF-811203, Oak Ridge National Laboratory (1982) (available from National Technical Information Service, United States Department of Commerce, Springfield, VA.)
[5] FURTH, H.P., BOOZER, A.H., The EST (ELMO Snaky Torus), personal communication (1982);
MILLER, R.L., Phys. Fluids **29** (1986) 1176.
[6] ROSENBLUTH, M.N., TSAI, G.T., VAN DAM, J.W., ENQUIST, M.G., Phys. Rev. Lett. **51** (1983) 1967.
[7] GRAWE, H., Plasma Phys. **11** (1969) 151.
[8] HOWARD, J.E., Plasma Phys. **23** (1981) 597.
[9] BATCHELOR, D.B., GOLDFINGER, R.C., Nucl. Fusion **20** (1980) 403, and references cited therein.
[10] BERNSTEIN, I.B., BAXTER, D.C., Phys. Fluids **24** (1981) 108.
[11] HAMASAKI, S., KRALL, N.A., SPERLING, J.L., Nucl. Fusion **23** (1983) 571.
[12] KILLEEN, J., KERBEL, G.D., McCOY, M.G., MIRIN, A.A., Computational Methods for Kinetic Models of Magnetically Confined Plasmas, Springer, New York (1986).
[13] KERBEL, G.D., McCOY, M.G., Phys. Fluids **28** (1985) 3629.
[14] GUEST, G.E., MILLER, R.L., CHANG, C.S., Nucl. Fusion **27** (1987) 1245.
[15] QUON, B.H., DANDL, R.A., DIVERGILIO, W., GUEST, G.E., LAO, L.L., LAZAR, N.H., SAMEC, T.K., WUERKER, R.F., Phys. Fluids **28** (1985) 1503.
[16] UCKAN, N.A., Phys. Fluids **25** (1982) 2381, and references cited therein.
[17] SUDAN, R.N., Phys. Fluids **6** (1963) 57.
[18a] CHU, K.R., HIRSHFIELD, J.L., Phys. Fluids **21** (1978) 461.
[18b] PRITCHETT, P.L., Phys. Fluids **29** (1986) 2919.
[19] GLADD, N.T., Phys. Fluids **26** (1983) 974;
HEDRICK, C.L., Convective-Absolute Boundary for Whistler Modes, Rep. ORNL-TM-3143, Oak Ridge National Laboratory (1970).
[20] GUEST, G.E., MILLER, R.L., CAPONI, M.Z., Phys. Fluids **29** (1986) 2556.

[21] STOTLER, D.P., BERK, H.L., ENGQUIST, M.G., Phys. Fluids **29** (1986) 1149, and references cited therein.
[22] GUEST, G.E., SIGMAR, D.J., Nucl. Fusion **11** (1971) 151.
[23] GUEST, G.E., DORY, R.A., Phys. Fluids **8** (1965) 1853; DORY, R.A., GUEST, G.E., HARRIS, E.G., Phys. Rev. Lett. **14** (1965) 131.
[24] TSANG, K., Phys. Fluids **27** (1984) 1659.
[25] HARRIS, E.G., J. Nucl. Energy, Part C, Plasma Phys. **2** (1961) 138;
KRALL, N.A., TRIVELPIECE, A.W., Principles of Plasma Physics, McGraw-Hill, New York (1973) 414 ff.
[26] FRIED, B.D., CONTE, S.D., The Plasma Dispersion Function, Academic Press, New York (1961).
[27] ABRAMOWITZ, M., STEGUN, I.A. (Eds), Handbook of Mathematical Functions, 10th edn, United States Government Printing Office, Washington, DC (1972) 889.
[28] LAU, Y.Y., CHU, K.R., Phys. Rev. Lett. **50** (1983) 243.
[29] GARNER, R.C., Electron Microinstabilities in an ECRH, Mirror-Confined Plasma, PhD Thesis; Rep. PFC/RR-86-23, Massachusetts Institute of Technology, Cambridge (1986).

(Manuscript received 2 March 1987
Final manuscript received 12 October 1987)

4. INTERACTIONS

Progress in achieving the Phase I objectives was enhanced through discussions with Dr. Joseph Santoru, of the Hughes Research Laboratories, and Dr. Marlene Rosenberg, of Jaycor. Dr. Santoru is active in an experimental program to characterize and exploit three-wave interactions in a novel microwave source concept; Dr. Rosenberg has provided a major portion of the theoretical support for the Hughes project. Both scientists provided pre-publication reports describing detailed experimental and theoretical results regarding the characteristics of the three-wave interaction and various parasitic phenomena. Their work, supported by AFOSR, has been valuable in demonstrating, at least in unmagnetized plasmas, the effectiveness of the three-wave interaction in generating electromagnetic radiation that is ideally suited for creating the magnetic-mirror confined hot-electron plasmas needed for amplification of whistlers.

5. PATENT DISCLOSURE

A patent application relating to this concept, "Method and Apparatus for Producing Intense Microwave Pulses" Serial No. 07/293,307, was filed on January 4, 1989.

6. RESEARCH PERSONNEL

The following personnel at Applied Microwave Plasma Concepts, Inc. are associated with the research effort:

1. Gareth E. Guest (Principal Investigator)
   Vice President (619)438-8244.

2. Raphael A. Dandl (Co-Principal Investigator)
   President (619)438-8244.

REFERENCES

1. see, for example, J. Jancarik, V. Kopecky, V. Piffl, J. Pohanka, J. Preinhaelter, M. Seidl, P. Sunka, and J. Ullschmied, "Generation and Heating of Plasma by Beam-Plasma Interaction", Proc. Third Conf. on Plasma Physics and Controlled Nuclear Fusion Research, IAEA (Vienna) 1968; I. Alexeff, G. E. Guest, D. Montgomery, R. V. Neidigh, and D. J. Rose, "Oscillations Present in Plasma-Electron Heating by an Electron Beam", Phys. Rev. Lett. 21, 344 (1968); and references cited in these two papers.

2. Tom Intrator, Noah Hershkowitz and Chung Chan, "Experimental Observation of Nonlinearly Enhanced $2\omega_{uh}$ Electromagnetic Radiation Excited by Steady-State Colliding Electron Beams", Phys. Fluids 27, 527 (1984); and references cited herein. Recent experimental and theoretical studies of the three-wave process in unmagnetized beam-plasma systems are described by R. W. Schumacher and J. Santoru, "Millimeter-Wave Generation via Plasma Three-Wave Mixing", June 1988. Annual report for the period 4/1/87 - 3/31/88 supported by AFOSR under contract F49620-85-C-0059 with Hughes Research Laboratory and M. Rosenberg and N. A. Krall, "Theory of a Millimeter-Wave Source Experiment", Annual Report J530-88-726/2472, May 27, 1988, Jaycor.

3. Preferential absorption of electromagnetic radiation by hot electrons was demonstrated experimentally by R. A. Dandl, H. O. Eason, P. H. Edmonds, and A. C. England, "Off-Resonance Effects on Electrons in Mirror-Contained Plasmas", Nucl. Fusion 11, 411 (1971); a recent theoretical analysis has been given by G. E. Guest and R. L. Miller in "Formation of Stable, High-Beta, Relativistic-Electron Plasmas Using Electron Cyclotron Heating", Nucl. Fusion 28, 419 (1988).

4. G. E. Guest and R. L. Miller, "Amplification of Whistler Waves Propagating Through Inhomogeneous, Anisotropic, Mirror-Confined Hot-Electron Plasmas", Phys. Fluids 31, 3690 (1988).

5. R. A. Dandl, "Method and Apparatus for Producing Microwave Radiation", U.S. Patent Number 4,733,133, March 22, 1988. See also, A. V. Gaponov-Grekhov, V. M. Glagolev, and V. Yu. Trakhtengerts, "Cyclotron Resonance Maser With Background Plasma", Sov. Phys. JETP 53, 1146 (1981).

REFERENCES (contd)

6. see, for example, B. H. Quon, R. A. Dandl, W. DiVergillio, G. E. Guest, L. L. Lao, N. H. Lazar, T. K. Samek, and R. F. Wuerker, "Impact of Multiple-Frequency Heating on the Formation and Control of Diamagnetic Electron Rings in an Axisymmetric Mirror", Phys. Fluids 28, 1503 (1985).

7. see, for example, Thomas H. Stix, "Energetic Electrons from a Beam-Plasma Overstability", Phys. Fluids 7, 1960 (1964)

8. E. G. Harris, "Plasma Instabilities Associated With Anisotropic Velocity Distributions", J. Nucl. Energy, Pt. C: Plasma Physics 2, 138 (1961).

9. T. M. O'Neil, J. H. Winfrey, and J. H. Malmberg, "Nonlinear Interactions of a Small Cold Beam and a Plasma", Phys. Fluids 14, 1204 (1971), and earlier work cited herein.

10. see, for example, Jon A. Davis and Abraham Bers, "Nonlinear Aspects of the Beam-Plasma Interaction", Polytechnic Institute of Brooklyn, Microwave Research Institute, Symposium on Turbulence of Fluids and Plasma, April 14-18, 1968, New York.

11. Edward G. Harris, "Classical Plasma Phenomena from a Quantum Mechanical Viewpoint", in Advances in Plasma Physics, W. B. Thompson, editor, John Wiley and Sons (New York) 1970.

12. see, for example, S. A. Kaplan and V. N. Tsytovich, Plasma Astrophysics, Pergamon Press, Oxford (1973); and B. Prasad, "Enhanced Coherent Raman Emission from Uniform Plasmas", Phys. Fluids 19, 464 (1976).

13. G. E. Guest and R. A. Dandl, "Microwave Heating Systems for Atmospheric Pressure Nonequilibrium Plasmas", Plasma Chemistry and Plasma Processing (1988).

14. G. E. Guest, R. L. Miller and C. S. Chang, "Formation of Relativistic Electron Plasma in Tokamaks using Electron Cyclotron Heating", Nucl. Fusion 27, 1245 (1987).

15. T. H. Stix, "The Theory of Plasma Waves", McGraw-Hill, New York (1962), Chapter 2.